Optical Property Optimisation of Lead Sulphide Quantum Dots

A THESIS SUBMITTED

BY

Guanran Zhang

FOR THE DEGREE OF

MASTER OF ENGINEERING SCIENCE

School of Chemical Engineering

The University of Adelaide

Adelaide, Australia

August 2013

DECLARATION

I certify that this work contains no material which has been accepted for the award of any other degree or diploma in any university or other tertiary institution and, to the best of my knowledge and belief, contains no material previously published or written by another person, except where due reference has been made in the text. In addition, I certify that no part of this work will, in the future, be used in a submission for any other degree or diploma in any university or other tertiary institution without the prior approval of the University of Adelaide and where applicable, any partner institution responsible for the joint-award of this degree.

I give consent to this copy of my thesis, when deposited in the University Library, being made available for loan and photocopying, subject to the provisions of the Copyright Act 1968.

I also give permission for the digital version of my thesis to be made available on the web, via the University's digital research repository, the Library catalogue and also through web search engines, unless permission has been granted by the University to restrict access for a period of time.

Signature: _____

Date: _____

ACKNOWLEDGEMENT

My eighteen months study at the University of Adelaide as a Master candidate has been enriched by the help of many people. Here I would like to take the opportunity to thank the people that had helped and supported me to make this thesis possible.

First and foremost, I would like to thank my supervisors Associate Professors Sheng Dai and Bo Jin (School of Chemical Engineering, University of Adelaide) for their great support and guidance over the past two years. During the numerous discussions with A. Prof Dai, his great theoretical and experimental knowledge had helped a lot in understanding and designing the project, experimental design and related knowledge understanding, and he's huge knowledge background has become a future goal for me to achieve. A. Prof Jin has always been willing to discuss with me on academic as well as personal matters. His suggestions on research study methods and future career planning have guided me through the whole post-graduate study.

I would also like to acknowledge Dr. Hu Zhang and Dr. Jingxiu Bi in our research group, both of whom have gave me generous help and valuable suggestions throughout the study. I would also like to thank Ms. Lijuan Wei, Leiyuan Guo, Masoumeh Zargar and Mr Bingyang Shi as well as other research group members from School of Chemical Engineering, University of Adelaide for their sincere help and useful suggestions. They are not only dedicating researchers to work with but also priceless personal friends. I learned a

lot working with these great people and it has been a real pleasure researching in this university.

This thesis was dedicated to my parents and grandparents in China, without whose love and support none of this would have been possible.

The thesis was written in memorise of my grandfather. May he have peace in the other world.

ABSTRACT

To improve photovoltaic performance, lead sulphide quantum dots (PbS QDs) have been introduced in the device structure. To achieve enhanced performance by using PbS QDs, it is essential to gain better understanding on the particle size control and surface modification. The aim of this thesis is to gain better understanding of the particle size control, growth kinetics and surface modification of PbS particles to reach optimised properties for possible future applications.

The particle size modification and growth kinetics were studied by systematically varying reaction parameters of reaction time, temperature and reactant feed to synthesize a series of PbS QDs with different first exciton peaks. Studying the absorption wavelength and the full-width-at-half-maximum of photoluminescence spectra from different reaction times shows the three-stage growth process from nucleation through particle growth to final size saturation of the QDs. For each of these stages, the particle size and growth rate were found to be determined by reaction temperature and the stabilizer oleic acid concentrations. By analysing the change of absorption peaks with these parameters, the activation energy of the particle growth stage was calculated.

A novel surface ligand exchange approach was explored. By attaching the Pb onto the desired ligand functional groups, the formed ‘atomic-ligand’ could be readily used for solution phase ligand exchange. Tridentate poly(ethylene glycol) methyl ether (mPEG)

was used as a model hydrophilic ligand for PbS exchange. The modification of mPEG was confirmed, and the atomic ligand exchange was compared with the conventional ligand exchange by TEM imaging and quantum yield measurement. The results showed quantum yield enhancement of 715% from 2.7% to 22% and particle dispersity in polymer via atomic-ligand exchange compared with traditional method.

In conclusion, the thesis demonstrated detailed kinetics study of PbS quantum dots during different particle growth stages. For the first time, activation energy for PbS quantum dots particle growth was reported to be 28.8kJ/mol. A novel ligand exchange approached was first proposed and the quantum yield was observed to enhance by 715% comparing to conventional exchange method. The results from this study provided important results on PbS QDs synthesis and optimization, which would largely facilitate further studies on the understanding of principle PbS QDs growth dynamics and surface modification using various functional groups.

TABLE OF CONTENTS

LIST OF FIGURES

LIST OF TABLES

LIST OF ABBREVIATIONS

AM 1.5	Air mass 1.5 distribution
BHJ	Bulk heterojunction
DMF	Dimethylformamide
DMSO	Dimethyl sulfoxide
DSSC	Dye-sensitized solar cell
DTPA	Diethylenetriaminepentaacetic acid
FF	Fill factor
FTO	Fluorine-doped tin oxide
FWHM	Full-width-at-half-maximum
HDA	Hexadecylamine
HOMO	Highest occupied molecular orbital
HSC	Heterojunction solar cell
ITO	Indium tin oxide
LUMO	Lowest unoccupied molecular orbital
MEH-PPV	Poly[2-methoxy-5-(2-ethylhexyloxy)-1,4-phenylenevinylene]
mPEG	Polyethylene glycol monomethyl ether
OA	Oleic acid
ODE	1-Octadecene
OSC	Organic solar cell
$PC_{61}BM$	[6,6]-phenyl-C61-butyric acid methyl ester
PCE	Power conversion efficiency
PEDOT:PSS	Poly(3,4-ethylenedioxythiophene) poly(styrenesulfonate)
PV	Photovoltaic
QD	QD

QE	Quantum efficiency
QY	Quantum yield
TEM	Transmission electron microscope
THF	Tetrahydrofuran
$(TMS)_2S$	Hexamethyldisilathiane
TOP	Trioctylphospine
TOPO	Trioctylphosphine oxide

Chapter 1 Introduction

1.1 Background

Since the successful industrialization of crystalline silicon-based solar cells, researches have been focusing on the fabrication and modification of photovoltaic (PV) devices to improve the power efficiency and reduce the production cost. In general, the development of solar cells has gone through three generations. The first generation was established by the Bell laboratories in 1954, which has the highest power conversion efficiency (PCE) approaching 30% by using crystalline silicon as semiconducting materials. The second generation is the dye-sensitized solar cells (DSSCs), which has lower prime cost, but the dyes suffer from degradation under heat and UV light, reducing device stability.[1,2] The third generation is the organic solar cells (OSCs) which uses thin films of organic material as semiconductors. These materials can be processed from solutions, and thus hold the promise of a simple roll-to-roll fabrication, leading to low-expense, large scale production. The research of organic solar cells has progressed rapidly in the past few years. Up to date, power conversion efficiency over 7.7% has been reported.[3]

The main problem for the OSCs is that undoped semiconducting polymers have fairly low charge mobility. While many inorganic semiconductors have charge carrier mobility of 10^{-1} to 1 cm^2/Vs, most conducting polymers only have carrier mobility around 10^{-6} cm^2/Vs,[4,5] resulting in short diffusion lifetime and recombination of the charge carriers.[6,7] Another issue is that the solar spectrum spans from 300 nm to as large as 2500 nm.

However conducting polymers very often have large band gaps, which limit their absorption spectra to the visible wavelength. Therefore, to improve the PCE for OSCs, band gap modification and charge carrier mobility enhancement are two major topics.[8,9]

Inorganic nanomaterials, especially PbS QDs, have been extensively studied in the past decades for their unique size dependent photoelectric properties, and these materials have seen various applications in OSCs. With band gap ranging from 1.77 to 0.69 eV, PbS QDs could absorb light in the near infrared wavelengths. Therefore, by combining the PbS QDs with conducting polymers, it could not only enlarge the absorption window, but the charge transfer could be potentially enhanced as well. Several studies on PbS QD-polymer heterojunction solar cells with PCE up to 3%[10-12] have been reported. In these cases, two principles should be considered for effective application of PbS QDs in polymer-based solar cells:

(1) The band gap of the nanoparticles should be modified to match that of the polymers for efficient charge transfer;
(2) The surface molecules of the nanoparticles should be functionalized to facilitate charge transfer and improve miscibility with polymers.

In order to optimise PbS properties for future application in PV devices, this thesis will be addressing these two principles separately.

1.2 Aim and objectives

The aim of this Master thesis is to optimise the optical properties of PbS QDs to meet the demand for the application of organic solar cells. To achieve such an aim, the thesis focuses on two major parts:

(1) Synthesize PbS QDs of different sizes to understand the particle growth mechanism and underlying kinetics;

(2) Investigate a novel approach for surface ligand modification to improve the quantum yield of post-ligand exchanged PbS QDs.

1.3 Outline of this thesis

Besides the *Introduction* (*Chapter 1*), *Literature Review* (*Chapter 2*) the *Materials and Methods* (*Chapter 3*) and the *Conclusions and Recommendation* (*Chapter 6*), two chapters focused on the above objectives are presented in this thesis.

Chapter 4, "*Synthesis, Size Modification and Kinetics Study of Lead Sulphide Quantum Dots*", focuses on synthesis and size control of the PbS QDs. By systematically investigating the change of absorption and emission spectra, the effect of reaction time, temperature and reactant feed ratio on particle growth are studied. The behaviour of particle growth with above parameters is further discussed to understand the underlying kinetics of the particle growth procedure and the particle growth activation energy is evaluated.

Chapter 5, "*Ligand Exchange of PbS Quantum Dots Using Tridentate Hydrophilic Polymer with Enhanced Quantum Yield*", introduces atomic-ligand exchange, a novel approach for ligand exchange. Carboxyl functionalized tridentate poly(ethylene glycol) methyl ether is chosen as a model hydrophilic ligand to investigate this approach. The key parameters to achieve such an approach are discussed. The successful exchange is confirmed by ^{1}H NMR, TEM, titration and the absorption and emission spectra. The atomic-ligand exchange approach is compared with conventional ligand exchange. The quantum yield (QY) measurements show eight-fold increase via the atomic-ligand exchange approach comparing with conventional one.

Chapter 2 Literature Review

2.1 Hybrid solar cells: structure and mechanism

Despite that solar cells have gone through a long journey of development, the basic structures within more or less remained the same. The main structure of any photovoltaic (PV) device comes down to four parts: anode, cathode, photoactive layer and external connection. Typically, a photovoltaic device uses transparent coated glass as one electrode and metal layer with high charge transfer efficiency as the other, in between is the semiconducting photoactive layer which plays the key role of converting photon energy to electric energy. Indium tin oxide (ITO) is the most commonly used transparent charge transfer anode material, which is coated as a thin film on top of the transparent substrate. A charge transfer layer is often coated on top of ITO to facilitate electron transfer to anode, therefore enhancing electrode performance. (Figure 2.1 A) The 'light to current' conversion takes place mostly within the photoactive layer. In a simplified charge transfer model (Figure 2.1 B), an electron on the highest occupied molecular orbital (HOMO) of the donor material absorbs the energy of an incident photon and is excited to the lowest unoccupied molecular orbital (LUMO). The excitation of the electron generates a positively charged hole on HOMO, such electron-hole pair is called an exciton. By carefully matching the band gaps between the donor, acceptor and the electrodes, the electrons and holes are further transferred into opposing electrodes. Thus, it is commonly

accepted that the effectiveness of the photoactive layer and the ability of charge transfer to opposite electrodes largely determine the overall efficiency of a photovoltaic device.

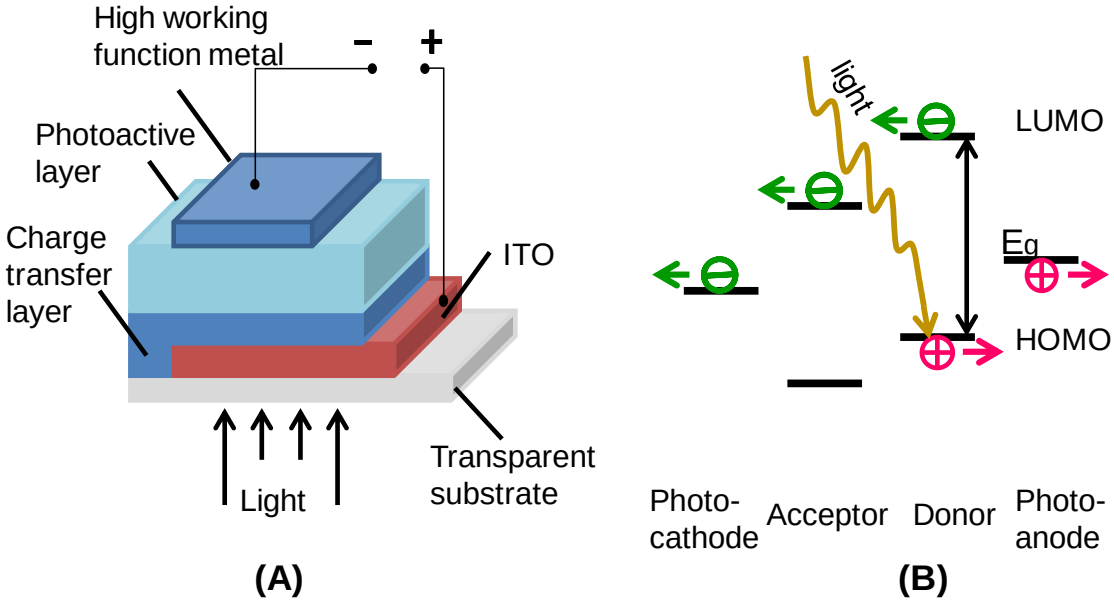

Figure 2.1 (A) Typical structure of a hybrid PV device; (B) the illustration of device working function. LUMO and HOMO are abbreviation for lowest unoccupied molecular orbital and highest occupied molecular orbital

Several important parameters are used to quantify the performance of PV devices. Quantum efficiency (QE) is termed as the fraction of the photons that are converted into excited charge carriers and are collected by the cell. In other words, QE represents the ability of a PV device to harvest photons. For inorganic PV devices, the quantum efficiency is usually close to 100%, while for a pristine organic semiconductor the QE is often below 1%.[8,9] For practical device characterization, the external quantum efficiency (EQE) is often used, which is the fraction of electrons penetrating an external circuit over the number of incident photons. Therefore the EQE includes transmitted and reflected photons. The open-circuit voltage (V_{oc}) and short-circuit current (I_{sc}) are the voltage and

current obtained when the cell is operated at the open circuit or short circuit modes. The V_{oc} and I_{sc} represent the maximum voltage or current possible for a PV device.[13] The fill factor (FF) is the ratio between the maximum power point of the cell to the product of Voc and I_{sc}, which in a manner determines the maximum power of a solar cell. Another important parameter is the power conversion efficiency (PCE). It is calculated as the ratio of the maximum output energy P_{max} to the incident light power Φ_e (the total energy input from incident photons on the device surface):

$$\mathrm{PCE} = \frac{\mathrm{P_{max}}}{\emptyset_{\mathrm{e}}} = \frac{\mathrm{FF \cdot Voc \cdot Isc}}{\emptyset \mathrm{e}} \quad (1)$$

To achieve high PCE, high QE is necessary; but a high QE does not necessarily guarantee high PCE. For standardized PV device characterization, solar simulator with light intensity of 1000 W/m^2 is commonly used. This is also termed as air mass 1.5 distribution (AM 1.5), corresponding to the sun's radiation coming from an angle of 48°.[14]

Since the investigation of ultrafast charge transfer between poly[2-methoxy-5-(2-ethylhexyloxy)-1,4-phenylenevinylene] (MEH-PPV) and buckminsterfullerene (C_{60}) by Sariciftci et al. in 1992,[15] the third generation of solar cells based on organic donor-acceptor has been intensively studied. The introduction of a C_{60} derivative [6,6]-phenyl-C61-butyric acid methyl ester ($PC_{61}BM$) solved the problems of low solubility and phase separation of C_{60}. $PC_{61}BM$ has since been widely used as the acceptor in OSCs.[16] Because of the exceptional optical and electrical properties as well as

thermal and chemical stability, polythiophene derivatives have become the most popular class of conjugated polymers in OSC application. State-of-the-art devices based on single-layered polythiophene: PCBM have PCEs exceeding 7%.[17-21] By applying a cathode interlayer[5] adopting an inverted cell structure[17] or combining two photoactive layers in a tandem cell,[22] the reported PCEs are getting closer to the commercial application threshold of 10%.[23] The energy levels of some commonly used organic semiconductors and their structures are summarized in Table 2.1 and Figure 2.2.

Table 2.1 Energy levels and band gaps of some common conducting polymers

	E_{LUMO} (eV)	E_{HOMO} (eV)	E_g (eV)
MEH-PPV[25]	-2.90	-5.30	2.40
MDMO-PPV[26]	-2.97	-5.33	2.36
P3HT[27]	-2.95	-5.12	2.17
PCBM[28]	-4.30	-6.10	1.80

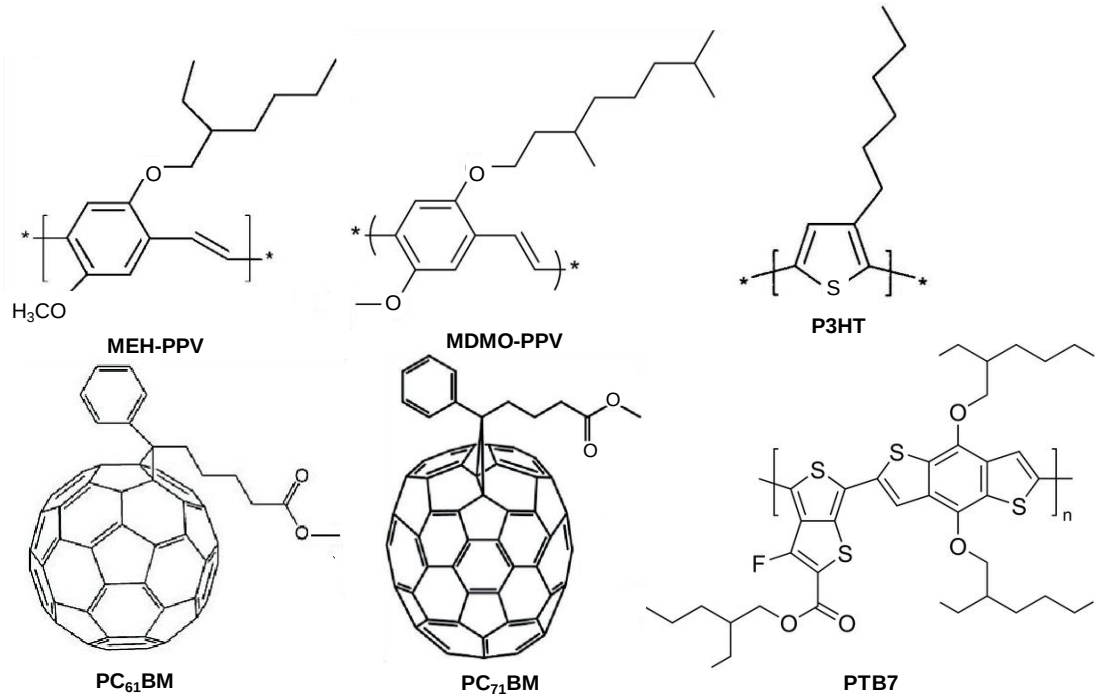

Figure 2.2 Structures of some common conducting polymers mentioned in this chapter

To push forward the OSC performance for commercial application, several key issues need to be investigated.

1) The small exciton diffusion length and low charge-carrier mobility limit the photoactive layer thickness below 100 nm,[24] this in turn limits the photon absorption of the solar cell.
2) The absorption window of organic semiconductors is narrow comparing to inorganic semiconductors,[25] hence confining the solar light utility.
3) For many of the above-mentioned devices, high PCE is only observed within a short period of time,[26] therefore improving device stability is crucial for commercialization.

In hopes of overcoming such obstacles, nano-structured inorganic materials have been introduced. Inorganic nanomaterials have versatility of different structures and sizes, which allow them to be further modified and decorated to obtain various functionalities.[27] The improving fabrication technology allows us to produce a whole range of semiconductor nanomaterials with zero-dimensional structure (or quantum dots),[28-35] one-dimensional structures (nanorods, nanowires, nanotubes and nanobelts),[34,36-40] two-dimensional structures (thin films or plates) [41,42] or even three dimensional structures (oriented arrays, continuous lattices).[43,44] These nanoparticles and nanostructures not only maintain good charge mobility as their bulk materials, in many cases their optical and electrical properties are size and structure dependent. By fabricating nanoparticles of desired materials and structures, their properties could be selectively engineered, allowing variation in material performance.[45]

PV devices with hybrid nanoparticle-conjugated polymer structure are termed as heterojunction solar cells (HSCs), since the photoactive layer of the PV device consists of at least two semiconductors with unequal band gaps. Typically two types of heterojunction structures have been adopted in the HSC designs: heterojunction bilayer and bulk heterojunction. Heterojunction bilayer solar cells (Figure 2.3 A) consist of two adjacent layers of donor and acceptor. For successful charge transfer, the layers need to be very thin to reduce recombination. Nonetheless, the ease of fabrication and structure simplicity makes bilayer devices helpful for evaluating the properties of new materials.[13] Bulk heterojunction (BHJ) solar cells could be disordered bulk heterojunction (Figure 2.3 B) or

ordered heterojunction (Figure 2.3 C). In either case, the electron donor-accepter interface has much larger surface area than heterojunction bilayer structure, and the mixture of donor and acceptor in nanoscale allows effective diffusion of excitons to the donor-acceptor interface thus largely decreasing charge carrier recombination.[46]

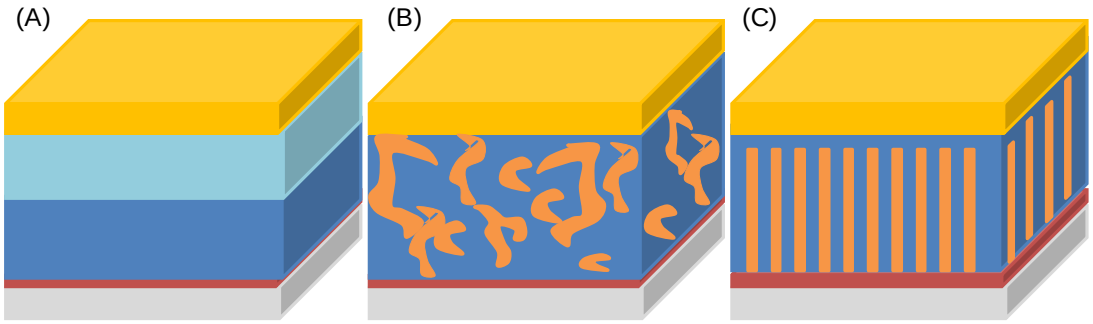

Figure 2.3 Schematic representation of (A) heterojunction bilayer, (B) disordered bulk heterojunction and (C) ordered bulk heterojunction structures

Problems for bulk heterojunction devices also exist, including the nanoparticles aggregation and phase separation between inorganic nanoparticles and conjugated polymer.[13,47] Therefore, surface modification for nanoparticles must be carefully designed for homogeneous mixing without trading off the charge transfer efficiency between donor and acceptor. The well designed structure of a PV device is the footstone for high performance; hence it is crucial to optimise photoactive layer structure and morphology for enhanced cell performance.

2.2 Application of inorganic nanoparticles

For organic solar cells, several nanomaterials have been introduced to fabricate nanoparticles-conjugated polymer heterojunction PV devices, including titanium dioxide (TiO_2), zinc oxide (ZnO), quantum dots (QDs) etc.[48] Many important studies have been done on topics of material synthesis and device modification.

2.2.1 Metal oxide

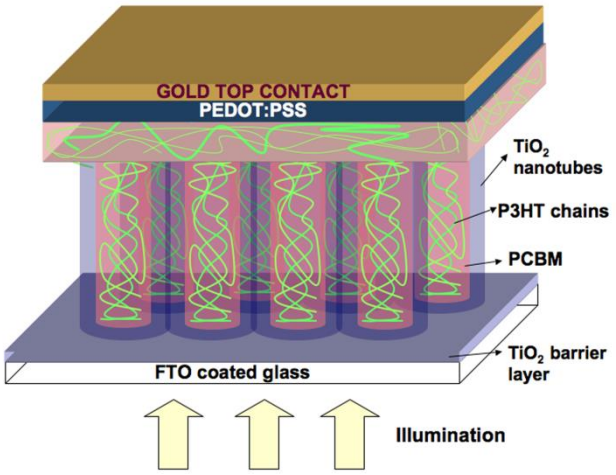

Figure 2.4 Illustration showing the device configuration, materials used, and the direction of illumination[49]

The application of titanium dioxide (TiO_2) and zinc oxide (ZnO) in organic solar cells generally falls into two types: charge-carrier transferrer and optical spacer. As electron transferrer, nanoporous or aligned nanotubes of TiO_2 and ZnO are commonly used. Figure 2.4 showed the application of aligned TiO_2 nanotubes in a P3HT/$PC_{71}BM$ device. Vertically aligned TiO_2 nanotube array was casted on fluorine-doped tin oxide (FTO)

casted glass substrate, with P3HT/$PC_{71}BM$ infiltrated into the nanotubes. This FTO/TiO_2 nanotubes/P3HT:$PC_{71}BM$/PEDOT:PSS/Au device reached 80% EQE at maximum absorption and PCE reached 4.1% at AM 1.5 illumination, indicating efficient charge generation and collection.[49]

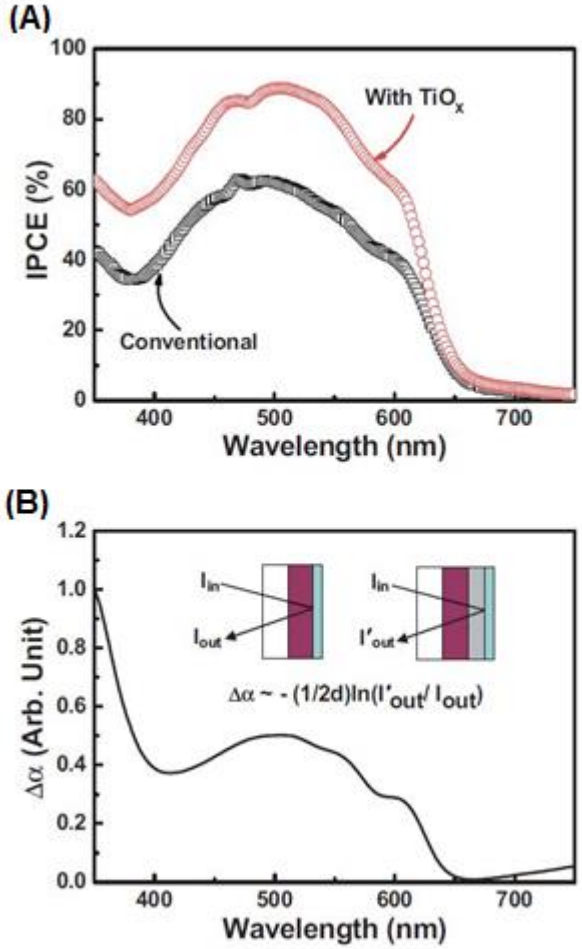

Figure 2.5 (A) Incident monochromatic photon-to-current efficiency for devices with and without TiO_x optical spacer; (B) the change of absorption spectrum resulting from the existence of optical spacer; inset: schematic of incident light beam path[50]

As optical spacer, a thin layer of metal oxide layer (around 30 nm in thickness) between the photoanode and active layer was applied. Kim et al.[36] compared devices with and

without this optical layer by measuring the reflectance spectrum. As could see in Figure 2.5, this spacer effectively redistributed incident light intensity and as a result, the number of carrier photon collected at the electrodes increased as well. The device fabricated using P3HT:$PC_{61}BM$ as active layer and ITO glass and aluminium as electrodes with this optical layer reached 5.0% efficiency at AM 1.5, which was more than double of a device without optical spacer (2.3%).[50]

2.2.2 Quantum dots

QDs are semiconductors whose electronic characteristics are largely related by the size and shape of individual particles. Due to the quantum confinement effect, when the size of a particle is compatible to the electron wave function, the energy state within the particle becomes incontinuous and the energy spectrum turns discrete. At this stage, the band gap of a particle is no longer that of the bulk material, it becomes size dependent. The relation between size and band gap of a spherical QD could be understood by Equation 2:

$$E_g^{nano} = E_g^{bulk} + \frac{\hbar^2\pi^2}{2r^2}\left(\frac{1}{m_e^*} + \frac{1}{m_h^*}\right) - \frac{1.8e^2}{\varepsilon r} \quad (2)$$

where E_g^{bulk} is the band gap of the bulk material, r is the radius for the spherical particle, m_e^* and m_h^* are the isotropic electron and hole mass, and ε stands for the electric permittivity of semiconductor. The second term in Equation 2 is the approximate particle-in-a-box confinement energy for an electron-hole pair in a spherical QD. The third term is the modified Coulomb attraction between electrons and holes. The Coulomb

attraction is comparatively small therefore negligible in qualitative discussion. Therefore, when size decreases the second term in Equation 2 increases, resulting in increase in particle band gap E_g^{nano}. By controlling the particle size, the band gap and optical properties of the QDs could be selectively modified for desired applications.

QDs of several II-VI and IV-VI semiconductors have been synthesized over the past two decades, among which lead sulphide (PbS) and lead selenide (PbSe) QDs, cadmium sulphide (CdS), cadmium selenide (CdSe) and cadmium telluride (CdTe) QDs are widely studied and have seen various applications. Table 2.2 lists the band gaps for some commonly used semiconductor bulk materials.

Table 2.2 Band gap of some semiconductor bulk materials

Bulk Material	**Band gap (eV)**
PbS[52]	0.41
PbSe[53]	0.27
PbTe[53]	0.29
CdSe[13]	2.10
CdTe[13]	1.95
ZnS[54]	3.6
TiO_2[55]	3.15
ZnO[56]	3.37

To obtain particles with desired size and properties, it is crucial to understand the growth of nanoparticles. The growth principle of QDs could be generally understood as a process of nucleation and particle growth.[51] The nucleation of solution-processed QDs is thermodynamically driven as the supersaturated solution is not energetically stable. The formation of new surface results in the change of overall free energy ΔG, which has a positive peak value in supersaturated conditions. The corresponding relation between particle size r and ΔG is illustrated in Figure 2.6. The nuclei have to reach a critical size r* to be thermodynamically stable as r* is corresponding to the maximum free energy change ΔG*. With particle size larger than r*, the ΔG would further decrease to form stable nuclei for further particle growth.

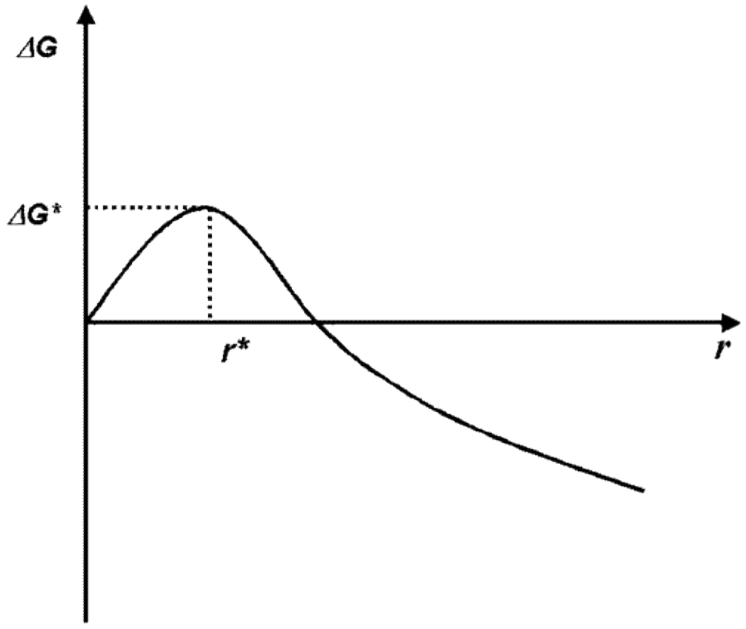

Figure 2.6 Illustration of free energy ΔG as a function of particle radius r[51]

Following the nucleation, particles grow by molecular addition until the equilibrium concentration is reached. Size-focusing also occurs at this stage. When the reactants are

depleted, Ostwald ripening takes place where smaller particles dissolve and larger particles continue to grow.[51] Bare nanoparticles are unstable in solution and often aggregate easily. Therefore for homogeneous dispersion the particle surface needs to be protected by a stabilizer. By controlling the amount of ligands in a reaction, the size and shape of the QDs could also be modified.[29] Organic ligands such as stearic acid (SA),[52] trioctylphosphine oxide (TOPO),[53] tetradecylphosphonic acid (TDPA),[54] hexadecylamine (HDA)[55] and several other aliphatic acids[56,57] have been used to successfully fabricate QDs of different sizes.

2.2.3 Cadmium chalcogenide quantum dots

Hot-injection synthesis method for Cd chalcogenide QDs was established in early 1990s. Murray et al. first introduced the high boiling point trioctylphosphine oxide (TOPO)/ trioctylphospine (TOP) system using dimethyl cadmium (Me_2Cd) as Cd source and trioctylphosphine chalcogenides (TOPE, E=S, Se and Te) as chalcogenide source.[58] They synthesized CdSe QDs which could be size-selectively precipitated by dropwise adding non-solvent into the synthesized QDs solution. Cadmium oxide (CdO) was used as Cd source instead of Me_2Cd due to the improved chemical and thermo stability and less toxicity.[59] Numerous publications have been published, mostly focusing on the control of QD size, morphology and optical properties. In one of the most cited Cd chalcogenide QD synthesis publications, the detailed experimental method for CdTe QDs was introduced. An amount of 0.4 mmol CdO and 0.8 mmol tetradecylphosphonic acid (TDPA) ligand

were dissolved in TOPO and heated to 300ºC in Argon to obtain Cd solution, which was then cooled to 270ºC. Tellurium of 0.52 mmol was dissolved in 2 g TOP to obtain Te stock solution, and this solution was injected into the hot Cd stock. The reaction temperature was then controlled at 250ºC until desired particle size was obtained.[60] CdTe QDs ranging from 2-8 nm in size were obtained from such method, and by further increasing precursor concentration nanorods could also be synthesized. The advantage of using CdO as Cd source is that lower reaction temperature is required due to its relatively low reactivity comparing to Me_2Cd. Also, the reaction is reproducible and suitable for large quantity synthesis because the reaction is less sensitive to the initial injection.

The effect of introducing TDPA into the reactant mixture was studied. By adding TDPA into the CdO/TOPO mixture and heating to desired temperature, the formed precursor was a mixture of Cd-TPDA and Cd-TOPO. Rapid colour change from colourless to yellowish took place in 2 minutes when the chalcogenide precursor was injected into the Cd precursor mixture. The Cd-TDPA/Cd-TOPO precursor was decomposed to Cd-TDPA only if the Cd precursor was cooled to room temperature and aged for a few days.[54,56] As a result, after reheating the aged Cd precursor to desired temperature and injecting chalcogenide precursor, the colour change took place in 4 minutes, indicating a slower nucleation procedure. The longer nucleation time was due to the reduced reactivity of Cd precursor Cd-TDPA comparing to Cd-TOPO, and as a result less nuclei were formed at the initial stage. Therefore by using TDPA as ligand more precursors would be available for further particle growth to reach desired size and shape. HDA was also used as the ligand

for Cd QD synthesis.[55] Using similar method as TDPA-TOPO-TOP synthesis described above, CdS, CdSe and CdTe QDs could be successfully synthesized.

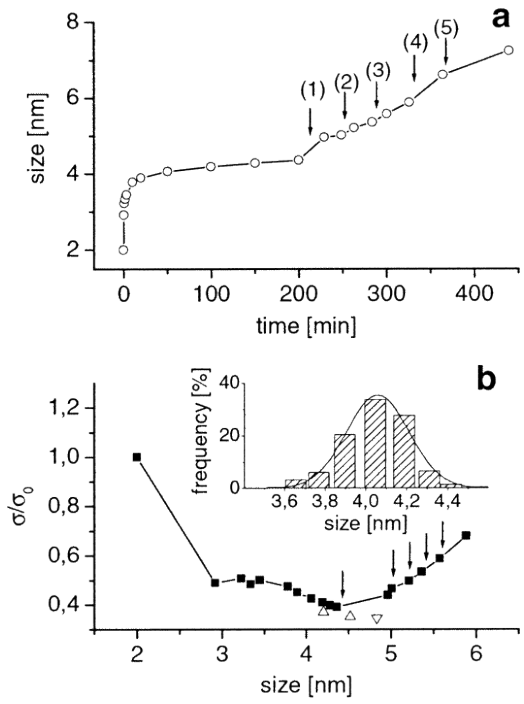

Figure 2.7 (A) Temporal dependence of average CdSe particle size at 300ºC (B) Particle size distribution of growing CdSe QDs: (■) during continuous growth at 300ºC; (Δ) obtained after stepwise growth (1 h 250ºC+1 h 280ºC) and (1 h 250ºC+1 h 280ºC+1 h 310ºC); (▼) obtained after slow additional injection of 0.4 mL of the stock solution at 280ºC to the stepwise grown nanocrystals. The inset shows a size histogram of CdSe nanocrystals with an average size of ~4.05±0.16 nm. Arrows indicate additional injections of stock solutions containing (1)-(3) 50%, (4) 100%, and (5) 140% of Cd and Se precursors compared to the initial amount of CdSe [55]

Particles of different sizes could be obtained by controlling reaction temperature and addition of precursors (Figure 2.7). The quantum yield of CdSe QDs with ~4 nm in diameter was reported to be 12%, which was a significant enhancement comparing to that of the CdSe QDs from TOPO-TOP system (9.6%).[55] Oleic acid was also investigated as the ligand for CdSe QD synthesis.[26] It was found that, the nucleation took place instantly

after Se precursor injection at 265ºC using oleic acid as capping ligand and 1-Octadecene (ODE) as solvent. An interesting observation was that at higher temperatures, the initial nuclei size 5 seconds after injection was smaller and the final particle size also became smaller. This was attributed to the increased nucleation rate at higher temperatures, resulting in smaller nuclei size and smaller final size. Another important observation was that by increasing the oleic acid concentration, the number of nuclei was almost linearly reduced and at the absence of oleic acid, nuclei sizes were larger than that in the presence of oleic acid. The function of oleic acid in the reaction was explained as two competing roles: as complexing agent it reduced the active monomer concentration, and it also capped the nuclei rapidly as they form. The dominating effect was believed to be the capping action at low ligand concentration. At high ligand concentration, the low monomer concentration would completely hinder the nucleation, resulting in a small population of nuclei and high concentration of remaining monomers. This would lead to an uncontrollable particle growth and wide size distribution.[56,61]

The particle size and optical properties could be post-synthesis modified as well, most commonly through the formation of a semiconductor shell outside the particle. By using different materials as shell, such core-shell nanoparticles could be classified into two types. Figure 2.8 illustrates the band gap for two types of core-shell particles. Type I core-shell nanoparticles have the wider band gap semiconductor as shell, and type II core-shell structure use semiconductors that have both LUMO and HOMO higher or lower than the core. Both types of core-shell particles could be synthesized by injecting shell precursor

solution into the core/stabilizer hot solution. Such method allows shell growth of several monolayers.[62-64]

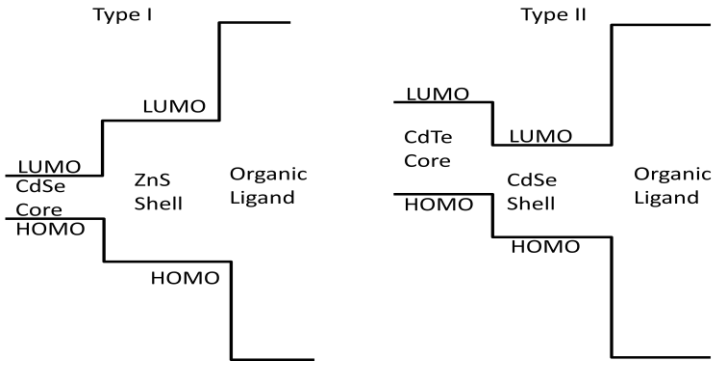

Figure 2.8 Illustration of band gap for type I and type II core-shell structures

For type I particles, the conduction band energy of the shell is higher than that of the core and the valence band energy of the shell is lower. The photogenerated electrons and holes are confined in the core material; therefore the stability and luminescence of the particles are largely improved without compromising the optical properties of core particle.[63,65] It has been reported that, by coating a ZnS shell on the as-synthesized CdSe core particles, the quantum yield increased from 12% of the core particles to 66% of CdSe/ZnS particles with ~1 monolayer shell thickness.[55] Such quantum yield increase was attributed to the successful surface traps passivation by shell formation. As for type II particles, because of the lower conduction band energy in one part and the higher valence band in the other, the exciton is effectively separated with one carrier in the core and the other in the shell. As a result, such core-shell particles would appear to have a larger band gap than either component material, making them attractive in PV applications.[64] In a previous report by S. Kim et al, modifying the coated CdSe shell thickness on as-synthesized CdTe core

particles could tune the band gap of the synthesized particles. For CdTe/CdSe particles with core size of 32 Å, by increasing the shell thickness from 11 to 24 Å, the photoluminescence spectra peaks red shifted from around 850 nm to around 920 nm.[64] However, the major problem for type II core-shell particles is that the particles showed reduced quantum yield below 4%, which was likely due to the spatial separation of charge carriers and unsuccessful charge separation during the exciton radiative lifetime.

2.2.4 Lead chalcogenide quantum dots

In recent years, more and more studies have been done on lead chalcogenide QDs and the application in PV devices. This is due to the small band gap of the bulk materials (Table 2.3), which gives possibility to synthesize nanoparticles which have absorption peak in infrared wavelengths that few other nanoparticles were found to have. Therefore establishing a controllable synthesis method is particularly important for particle size modification. As the most studied Pb chalcogenide QDs, lead sulphide QDs will be discussed as a representative. Early synthesis methods of monodispersed PbS QDs date back to 1990, where H_2S gas was injected into lead acetate solution with poly(vinyl alcohol) as stabilizer. Average diameter of 40 Å was reported, however the use of gas reactant limited the application of such method.[27] Synthesis methods on substrates and in gas phase were also proposed, but such methods did not allow one to fine tune the particle size, and thus limiting further application.[37]

Table 2.3 Size and band gap of some synthesized QDs

Material of quantum dots	Range of particle size(nm)	Band gap (eV)
CdSe[10,56]	3-14	2.43-1.91
CdTe[69]	2.5-5.1	2.3-1.95
PbS[70]	2.5-7	1.77-0.69

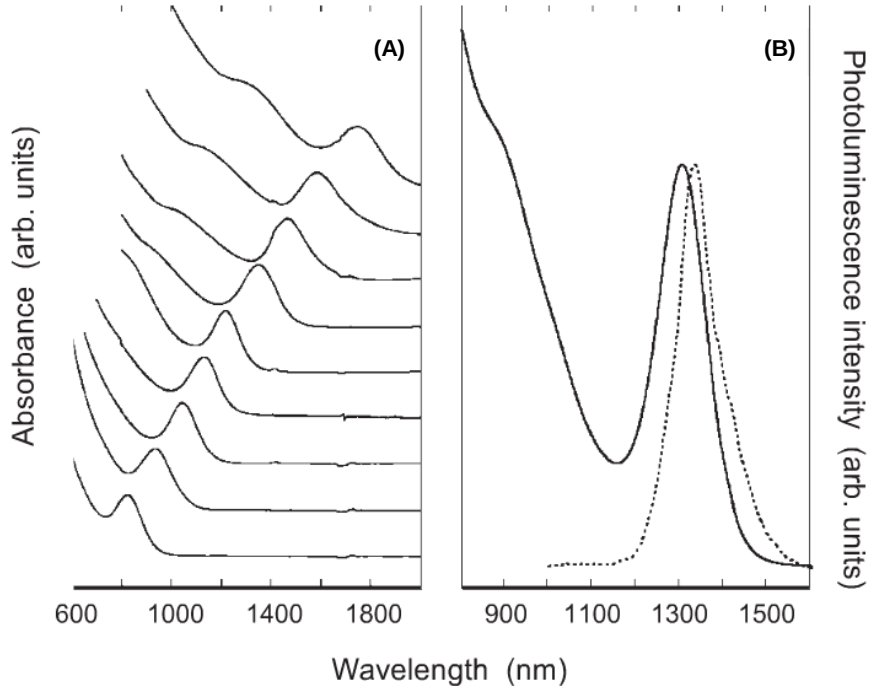

Figure 2.9 (A) Absorption spectra of size-tunable PbS QDs spanning in the near-infrared region; (B) Absorption and photoluminescence peaks for a sample of ~6.5 nm in diameter [57]

A mature hydrothermal method was first reported in 2003 by Hines and Scholes,[57] which was derived from the synthesis of cadmium QDs and lead selenide QDs. They used an organic lead salt lead oleate as lead precursor, an organic sulphur compound hexamethyldisilathiane ($(TMS)_2S$) as sulphur precursor and ODE as solvent. As shown in Figure 2.9 A, a range of PbS QDs with their absorption peaks from 800 nm to 1700 nm

were synthesized, and the full-width at half maximum (FWHM) of the photoluminescence spectrum in Figure 2.9 B was around 100 meV (~111 nm calculated from figure). They found that after injecting the S precursor into the Pb oleate solution nucleation takes place instantly, similar to the phenomenon observed for CdS QDs.[61] But unlike cadmium QD synthesis, increasing the concentration of OA didn't appear to have much effect on the success of nucleation, which was attributed to higher reactivity of $(TMS)_2S$ comparing to chalcogenide elements used for most Cd QD synthesis. A striking behaviour of size-narrowing was observed for PbS QDs. As shown in Figure 2.10, after separating synthesized QDs from the reactant solution and redispersed in pure solvent the nanocrystals were found to undertake size redistribution especially in the first 12 hours where a blue shift in absorption peak and decrease in FWHM was observed. Similar phenomenon has also been reported for gold nanoparticles. The mechanism was explained to be the combination of a heat-induced digestive ripening where larger particles break apart and smaller particles increase in size and the etching of excess ligand on particle surface. Such explanation might not be suitable for PbS, since the size focusing took place at a room temperature and excess ligand was removed from the sample solution.

Figure 2.10 (A) Absorption spectra of a single PbS nanoparticles sample in toluene at time intervals up to 96 hours, indicating a size-focusing after synthesis; (B-C) TEM images of the nanocrystals solution taken immediately after synthesis (B) and 24 hours after synthesis (C) [57]

The advantages of Scholes' method included the ease of particle size control via different reaction parameters, the easy precipitation of synthesized particles and well dispersity in several organic solvents. This method also allowed relatively high conversion rate, as the sulphur precursor $(TMS)_2S$ is a very active compound comparing to the sulphur element, and reactions using $(TMS)_2S$ always tend to deplete the sulphur precursor. The fluorescence quantum yield was around 20% for their sample with 6.5 nm diameter using NIR standard dye IR125 as reference. This method has since been widely used and adopted by researchers. Many studies have been done to understand the synthesis process and particle growth of PbS QDs.

A later study further investigated different parameters during PbS QD synthesis.[57,66] They first explored several S sources. Three S sources were used to synthesize PbS QDs, namely $(TMS)_2S$, thioacetamide (TAA) and element S. It was observed that both $(TMS)_2S$ and TAA could be used in QD synthesis with narrow absorption peak, however for element S reaction only took place at temperature above 180ºC and particles were soon aggregated. $(TMS)_2S$ showed better reactivity as the reaction could readily take place at room temperature, while for TAA temperature above 40ºC was necessary. It was also observed that while TAA could be used to fabricate QDs with good adsorption, the photoluminescence spectrum was poor. While using $(TMS)_2S$ as the S source, by increasing reaction temperature from room temperature to 120ºC under constant reactant concentration, the absorption peak gradually red shifted from 633 to 859 nm. The absorption peak showed a few nanometres increase with relatively constant FWHM of photoluminescence spectra of around 100 nm when increasing reaction time from 6 minutes to 4 hours. Different reactant concentrations and reactant feed ratios were compared as well. By increasing the S concentration from 0.0175 M to 0.0350 M with constant reactant feed ratio, the first exciton wavelength of the absorption spectra showed significant decrease, especially at a temperature above 50ºC. Further increasing S concentration from 0.0350 M to 0.0700 M didn't show any significant effect on absorption wavelength, but with higher concentration the change of first exciton wavelength with temperature appeared more linear. Different molar ratios between oleic acid-PbO and PbO-$(TMS)_2S$ were investigated with fixed S concentration at 0.0350 M. For oleic acid-PbO feed, by increasing the OA-PbO ratio from 2:1 to 4:1 increase in first exciton

wavelength was observed, but further increasing the OA-PbO ratio from 4:1 to 16:1 didn't show as significant effect on first exciton wavelength. Increasing the PbO-$(TMS)_2S$ ratio from 2:1 to 4:1 showed little effect on absorption peak wavelength. Further increasing the ratio to 8:1 significantly increased peak wavelength at a temperature higher than 90ºC, though no information on peak wavelength at ambient temperature at such ratio was given. The authors therefore drew a conclusion that increasing OA-PbO ratio would result in increasing absorption peak wavelength due to improved reaction medium solubility. Little information on how peak wavelengths change with OA amount was given. The synthesized particles showed good stability over 2 months period, and little photo-oxidation was observed. Another study by the same group reported on the effect of reaction time on absorption peak wavelength.[67] They reported a size-focusing stage during which the absorption peak wavelength remained relatively constant. After this stage the Ostwald ripening would occur, causing further increase of peak wavelength.[67] Little support on such observation was available for PbS and Cd chalcogenide QDs. Also, Ostwald ripening of nanoparticles does not necessarily need elevated temperature.[68] Therefore, it is somewhat questionable about the formation of such size-focusing particles.

For application of PbS QDs in PV devices, the particle size control is important to obtain particles with desired optical properties. However, up to now the synthesis of PbS QDs for solar cell application was mostly based on reported absorption spectra and fixed recipe. Despite that a few studies have demonstrated general relation tendencies between reaction conditions and particle property, the reported studies up till now were still ambiguous on

particle size control and underlying kinetics. Therefore, further study on the effect of different reaction conditions on particle size and size dispersity, and reaction kinetics for PbS QD synthesis is necessary.

2.2.5 Ligand exchange for quantum dots

For the synthesis of lead sulphide QDs with narrow size distribution, oleic acid is most commonly used as the surface ligand.[57] While effective as stabilizer during synthesis, the oleate ligand narrows the nanoparticles solubility to only several organic solvents like toluene and chloroform, limiting further applications in other solution environments. It has also been found that, when blending PbS QDs with MEH-PPV, under 200 mW illumination no detectable photovoltaic response was observed. However when using octylamine capped QDs, photocurrent of around -2.0 μA was observed at -1 V bias, which was 160 times that of oleic acid capped particles. This was attributed to the decreased chain length from 18 carbons for oleic acid to 8 carbons for octylamine. The reduced chain length decreased the barrier at the particle/polymer interface for exciton dissociation and also improved charge transfer within the nanoparticles phase.[69] Therefore it is important to replace them with other electroactive organic molecules through a procedure called ligand exchange before applying PbS QDs in photoelectric devices.

The common ligand exchange strategy for PbS QDs is mixing largely excess amount of desired ligand molecules and OA-capped PbS QDs in solution and vigorously stir or ultrasonic for a period of time. During this process, some of the OA ligands would break

off the nanoparticles surface, thus allowing the attachment of other ligands. Therefore it is necessary to ensure the excess amount of new ligand, as one could theoretically assume that if reaction time is long enough, the ratio of new ligand to OA on QD surface should be in agreement to the ratio between initially added new ligand amount and total OA amount on particle surface. It could also be concluded that multiple attachment is preferred comparing to single attachment between ligand and nanoparticles.

Based on such requirements, a few strategies are available for ligand design. For PV applications, short chain ligands are commonly used for a better charge transfer.[70] Table 2.4 lists some exchanging ligands that have been used. Bilinkers with two thiol groups on both ends of the molecules were used for casted film treatment.[71] When transferring QDs to a more polar solvent, large molecules are often used to improve solubility. Polymers with multiple functional groups are widely studied for ligand exchange, as comparing to monodentate polymer multidentate ligands showed significantly increased ligand exchange yield.[72] Ligand exchange for QDs have been carried out using poly(acrylic acid)[54] and poly(N-isopropylacrylamide)[73] to form core-shell or corona structured particles with good dispersity in alcohols.

Table 2.4 Some commonly used functional groups and ligands for QDs ligand exchange

Functional group	Ligand used	References
Thiol group	Thiol-functionalized poly(ethylene glycol)	71
	3-mercaptopropionic acid	79
	Dithiocarbamate	80
	11-mercaptoundecanoic acid	78
Carboxyl group	Poly(acrylic acid)	72, 73
	Functionalized PEO-PCL-PEI bulk copolymer	81
	Aliphatic acids	82
	Carboxyl-functionalized fullerene	76
Amino group	oleyamine, hexylamine	83-85
	n-butylamine	70
Pyridine, Porphyrin	p-(dimethylamino)pyridine	86
	tetra-meta-pyridyl porphyrin	87

As listed in Table 2.4, various functional groups, including thiol group,[51] carboxyl group[52,54] and dithiocarbamate,[59] could be used for ligand exchange due to the strong bonding between Pb-S and Pb-O atoms. Thiol group-containing ligands are particularly popular for solar cell applications,[70,74,75] as they act as good photoluminescent quenchers for QDs. It was reported that the quenching efficiencies depend on the size and charge of the molecules.[74] For the commonly used thiol containing ligands, the quenching efficiency

decreases with increasing chain length, in the order of mercaptoacetic acid > mercaptobenzoic acid > β-mercaptoethanol > mercaptoundecanoic acid. It should be noticed that functionalizing the desired ligand allows many compounds to be used for ligand exchange, but the solvent stability and optical properties of exchanged QDs could be compromised by shortening the ligand chain length and stripping off the original oleic acid ligand. Precipitation after ligand exchange under illumination often occurs,[71] rendering the applicability of some ligands.

A major problem for the ligand exchange method above is that the quantum yield of QD particles is often significantly decreased after exchange reaction. There are two possible reasons for this: the surface oxidation of nanoparticles during the ligand exchange reaction and the surface etching caused by the loss of oleic acid ligands. The surface oxidation results in the formation of large band gap oxidation layer on the surface of PbS nanoparticles, resulting in fluorescence quenching and insulation of photogenerated charge inside the particle. The surface etching refers to that when the ligand dissociates from the particle surface, a parallel dissociation of Pb-ligand unit is also possibly taking place. This is due to the comparable binding energy between Pb-carboxylate group and Pb-S atoms on a highly curved QD surface.[76] As a result, the absent of Pb atoms in crystallite surface leaves deep level surface traps, compromising the particle performance.

To solve such problems, a few possible solutions were proposed. In 2011, a ligand exchange strategy was reported using Pb^{2+} cation attached ligands.[77] By reacting PbO with

the desired carboxylic ligand which was very similar to the preparation of Pb precursor for PbS QD synthesis, an organic Pb salt could be obtained. The Pb^{2+} cation could readily fill in the vacancy caused by OA detachment when using such attached ligands for ligand exchange. Only 4% loss in quantum yield was observed for the reported experiments using C8 and C12 aliphatic ligands.[77] Sargent's group recently reported another effective surface trap passivation route. [78] They introduced a cadmium halide salt during PbS QDs synthesis, and the halide atoms filled into the empty trenches on particle surface. The calculated density of state showed a decrease in hybrid passivated particles comparing to unpassivated QDs, further leading to a significant increase in power conversion efficiency of fabricated solar cells.[78]

PbS QDs have small band gaps from 0.69 to 1.77 eV, while most conjugated polymers and other semiconductors have band gaps above 1.0 eV. These small band gap QDs could absorb solar spectrum in the near infrared region and infrared region while polymer semiconductors couldn't. Therefore blending PbS QDs with conducting polymers makes it possible to further increase quantum efficiency thus holds a promise in reaching higher PCE. Several researchers have used PbS QDs in organic-based solar cells. In 2007, Günes et al used PbS QDs and P3HT to fabricate a bilayer solar cell with PCE of 0.04%.[10] In 2010 devices with PbS and PCBM bilayer structure were fabricated.[79] The PbS layer was annealed under different conditions, and the air annealed device showed increase in both I_{sc} and V_{oc} comparing to nitrogen annealed device, indicating an oxygen-induced reaction in air. The authors concluded that during air annealing, an oxidized layer of PbO, $PbSO_3$ and

$PbSO_4$ was formed on the QD surface. The wider band gap of the oxides prohibited charge carrier recombination thus resulting in results in a better performance. They also fabricated a device with fast ozone-treatment (6 s at room temperature) of PbS layer, which showed the highest performance with PCE of 1.68% comparing to PbS layer annealed under N_2 or air (Figure 2.11).[79]

It is also possible to directly synthesize QDs in the conducting polymer matrix. PbS QDs were synthesized using traditional method, and poly(2-mehothoxy-5(2-ethyl)-hexoxy-p-phenylenevinylene (MEH-PPV) was dissolved in the Pb precursor prior to S precursor injection. The existence of the polymer offered nucleation site for crystallization, which also lowered the rate of particle growth.[80]

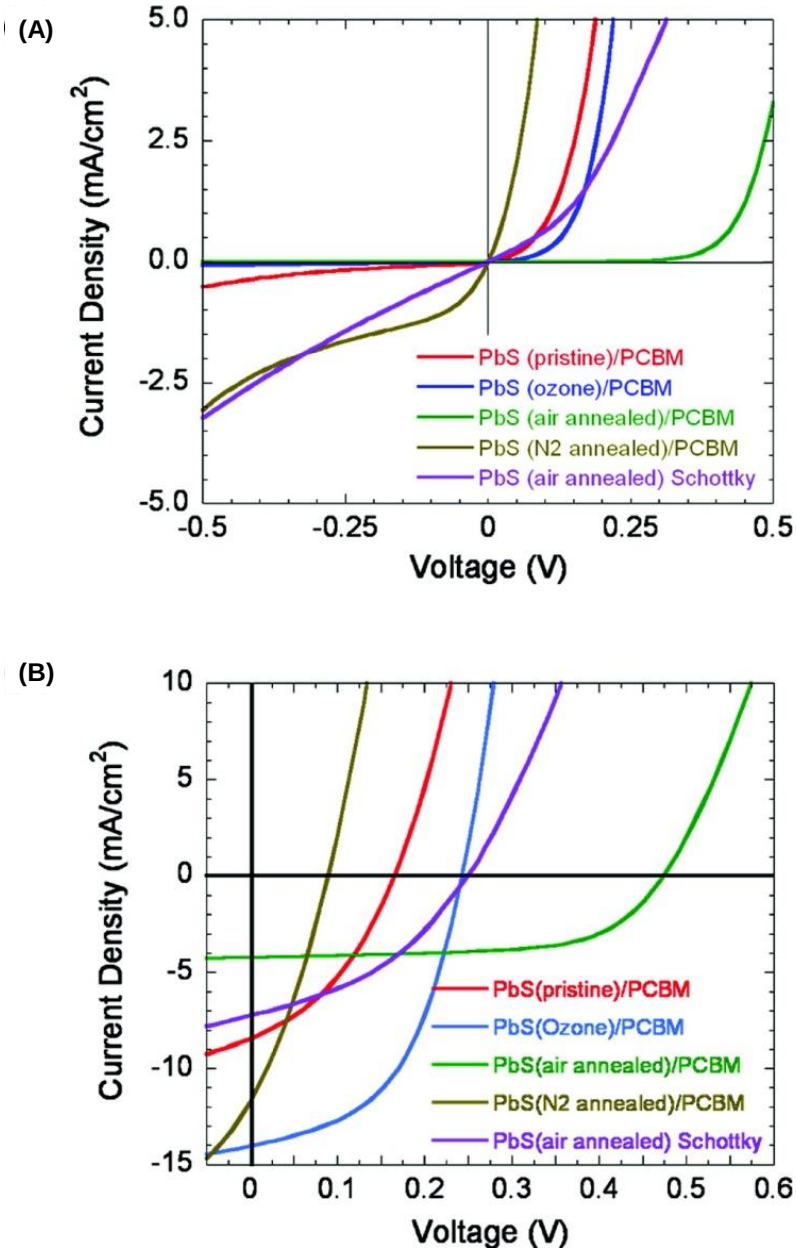

Figure 2.11 Current-voltage characteristics of PbS/PCBM solar cells (A) in the dark and (B) under AM 1.5 illumination [79]

2.3 Summary

To improve the performance of the organic-based solar cells, various studies have been done on semiconducting polymer modification and cooperating inorganic nanomaterials to fabricate heterojunction solar cells. Nanostructured materials, including TiO_2, ZnO and several semiconductor QDs have been applied, among which the QDs, particularly PbS QDs, holding great potential in device efficiency improvement due to the size tunability and outstanding optical properties. Size-monodispersed QDs have been successfully fabricated, and several synthesis parameters have been found to play important roles in controlling particle size, namely reaction time, temperature and reactant feed. The underlying mechanism for particle growth still requires a better understanding.

For application in PV devices, the oleic acid-capped PbS QDs need to carry out ligand exchange to replace oleic acid with other functionalized ligands for better solubility and charge transfer. Many studies have been done on the ligand exchange for QDs. A major problem is that most ligand exchange processes result in significant decrease in quantum yield. Several QD-polymer heterojunction devices have been fabricated, yet the power conversion efficiency was considerably low, possibly due to insufficient charge transfer and short carrier lifetime.

Hence, we conclude that for application in polymer-based solar cells, it is essential to (1) have a better understanding of particle growth kinetics and particle size modification and

(2) improve the current ligand exchange methods to improve optical properties and surface chemical properties for further PV application. These are the two main research objectives investigated in this thesis study. Results and discussions are presented in Chapters 4 and 5.

Chapter 3 Materials and Methods

3.1 Materials

Lead (II) oxide powder (PbO; ≥99.9% trace metals basis), Hexamethyldisilathiane ($(TMS)_2S$; synthesis grade), Oleic acid (OA; ≥99%), 1-Octadecene (ODE; 90%), Polyethylene glycol monomethyl ether (mPEG; Mn=5000), Diethylenetriaminepentaacetic dianhydride (DTPA dianhydride; 98%), Zinc phthalocyanine (dye content 97%) and 1-Octadecene (ODE; 90%) were purchased from Sigma-Aldrich. Sulphuric acid and all organic solvents were purchased from Scharlau. 1-Octadecene was distilled before use, azeotropic distillation was carried out for the purchased mPEG before further use. All other chemicals were of analytical grade and used as received. Deionized water (MilliQ water, 18.2 $M\Omega \cdot cm^{-1}$) used in all reactions was obtained from an EASY pure II ultrapure water purification system.

3.2 Synthesis methods

3.2.1 PbS quantum dot synthesis

The lead sulphide (PbS) QDs synthesis method was derived from previous report by M. Hines and G.D. Scholes.[57] Schlenk line and flasks were used in all synthesis reactions and the whole system was either argon filled or under vacuum to ensure oxygen free environment. In a typical reaction, 89.3 mg (0.4 mmol) of PbO, 0.317 mL (1 mmol) oleic

acid and 3.65 mL of 1-octadecene (ODE) were added into a Schlenk flask and heated to 150ºC for 1 hour in argon environment to obtain clear yellow solution. Then the heating mantle was adjusted to desired temperature for QD synthesis, the solution was heated for at least 30 minutes until temperature stabilized. 0.042 mL hexamethyldisilathiane ($(TMS)_2S$, 0.2 mmol) and 2 mL ODE were transferred into another Schlenk flask under argon protection; the clear mixture was then treated by freeze- pump-thaw degassing three times to remove remaining oxygen. The $(TMS)_2S$ solution was quickly injected into the Pb oleate solution under heating condition. Magnetic stirring was controlled at 250 rpm throughout the reaction. Change of solution colour was immediately observed, turning from clear yellow to dark brown in a few seconds. During the QD synthesis, samples were taken with argon-purged syringes at different time to monitor particle growth.

All samples were washed as follows: 0.5 mL of taken sample was immediately added to 15 mL of acetone and centrifuged at 12000 rpm for 3 minutes to precipitate the obtained PbS QDs. The clear supernatant was discarded. The dark precipitant was dispersed in 2 mL of toluene and added with 13 mL of acetone. The mixture was centrifuged at 12000rpm for 4 minutes. This procedure was repeated at least 3 times to ensure complete removal of remaining reactants. The final precipitant was dispersed in 4 mL toluene and kept in brown-tinted glass vials with aluminium foil wrap. For long term storage, the samples were again purged with argon and kept at -20ºC.

3.2.2 Synthesis of tri-dentate mPEG

Dried mPEG of 5 g was added into a glass vial (with magnetic stirrer inside) containing 10 mL THF and heated in 50ºC water bath until completely dissolve. The solution was cooled to room temperature in air, and then 200 mg DTPA dianhydride (slightly over 1:2 in molar ratio to mPEG) was added into the mPEG solution. The solution was stirred until DTPA solid was dissolved completely, and 4 drops of concentrated H_2SO_4 were added into the solution as the catalyst. The reaction flask was then sealed with cap and parafilm and stirred in 50ºC water bath for 5 hours. The modified mPEG was precipitated by adding into large amount of diethyl ether dropwise. The precipitated polymer was separated by filtration and dried in 50ºC oven. The polymer was washed with diethyl ether three times to ensure complete removal of sulphuric acid and unreacted DTPA. The obtained polymer was white in colour.

3.2.3 Attaching Pb atom onto carboxyl groups for atomic-ligand approach

An amount of 1 g DTPA decorated mPEG was redissolved in 5 mL DMF in a Schlenk flask in 50ºC water bath. 40 mg PbO was added into completely dissolved polymer solution, and the mixture was stirred in 110ºC oil bath for 3 hours. After cooling to room temperature, the mixture was centrifuged at 10000 rpm for 4 minutes to remove unreacted PbO powder. The supernatant was further centrifuged twice to obtain clear yellow solution

of mPEG-DTPA-Pb in DMF. The mPEG-DTPA-Pb was precipitated with diethyl ether twice and dried in oven.

The above process was also carried out at 50ºC to compare the effect of temperature.

3.2.4 Atomic-ligand exchange

The obtained PbS QDs were dissolved in toluene to obtain clear solution at 1.954 mg/mL for further ligand exchange reactions. 0.1 g Pb attached tri-dentate mPEG was dissolved in 2 mL DMF in a Schlenk flask with magnetic stirrer. The flask was heated in 50ºC oil bath until all solids were dissolved, then the solution was degassed three times by freeze-pump-thaw method to remove dissolved oxygen. The flask was filled with argon after degasification. The solution was then heated to 110ºC, and 2 mL PbS QDs solution was injected into the heated flask using an argon flushed syringe. The exchange reaction was allowed for 2 hours. After reaction, the sample was precipitated with large amount of diethyl ether three times and dried in argon.

The above method was also carried out at 50ºC to compare the effect of reaction temperature.

3.2.5 Conventional ligand exchange approach

The DTPA modified mPEG ligand exchange was also carried out via conventional ligand exchange method. 1 g of tri-dentate mPEG sample without Pb atom attachment was added in 2 mL DMF and heated in 50ºC water bath until all solids were completely dissolved. 2 mL PbS QD solution was then added into the solution. The mixture was kept in ultrasonic bath for 2 hours. The particles were precipitated with diethyl ether three times and dried in argon.

3.3 Characterization

Absorption spectra were measured with Shimadzu UV-1601 UV–VIS Spectrophotometer. All QD samples were characterized immediately after synthesis to reduce the effect of self-ripening. The fluorescence spectra of synthesized particles were measured with Shimadzu RF-530/PC Spectrofluorometer. Both spectra were measured using quartz cuvettes. Transmission electron microscope (TEM) images were taken using PHILIPS CM 200 Transmission Electron Microscope. TEM samples were prepared as follows: 1 drop of diluted sample solution was dropped onto the copper mesh using a 20 μL pipette. The copper mesh was held in air overnight to ensure complete evaporation of solvent and then used for measurement. Hanna HI 8733 conductivity meter and TPS AQUA-P V7694 pH meter are used for titration of modified mPEG before and after PbO reaction. 1H NMR spectra were taken using Varian Inova 600 MHz NMR system.

Chapter 4 Synthesis, Size Modification and Kinetics Study of Lead Sulphide Quantum Dots

4.1 Nucleation and particle growth

To understand the process of particle growth for PbS QDs, a series of samples were taken during the reaction process with molar ratio between oleic acid, PbO and $(TMS)_2S$ to be 5:2:1 at the reaction temperature of 50°C. The samples were further analysed by UV-Vis spectrophotometer. Figure 4.1 shows the absorption and emission spectra for the samples taken at different reaction time. The wavelength of first exciton peak increases from 510 to 666 nm as seen in Figure 4.1 A. Fluorescence spectra in Figure 4.1 B were obtained corresponding to the first exciton peaks. The shift in fluorescence spectra also proves the increase in particle sizes. The full-width-at-half-maximum data (FWHM) were calculated from the fluorescence spectra, with average FWHM of 68.1±2.5 nm, indicating good size uniformity. It is also noticed that FWHM (70.5 nm) in the first sample which was taken immediately after the injection of S precursor is significantly larger than that of other samples. Ignoring the first sample, the other samples have an average FWHM of 68.0±1.0 nm. The TEM images (Figure 4.2) confirmed the near spherical shape and size of synthesized QDs.

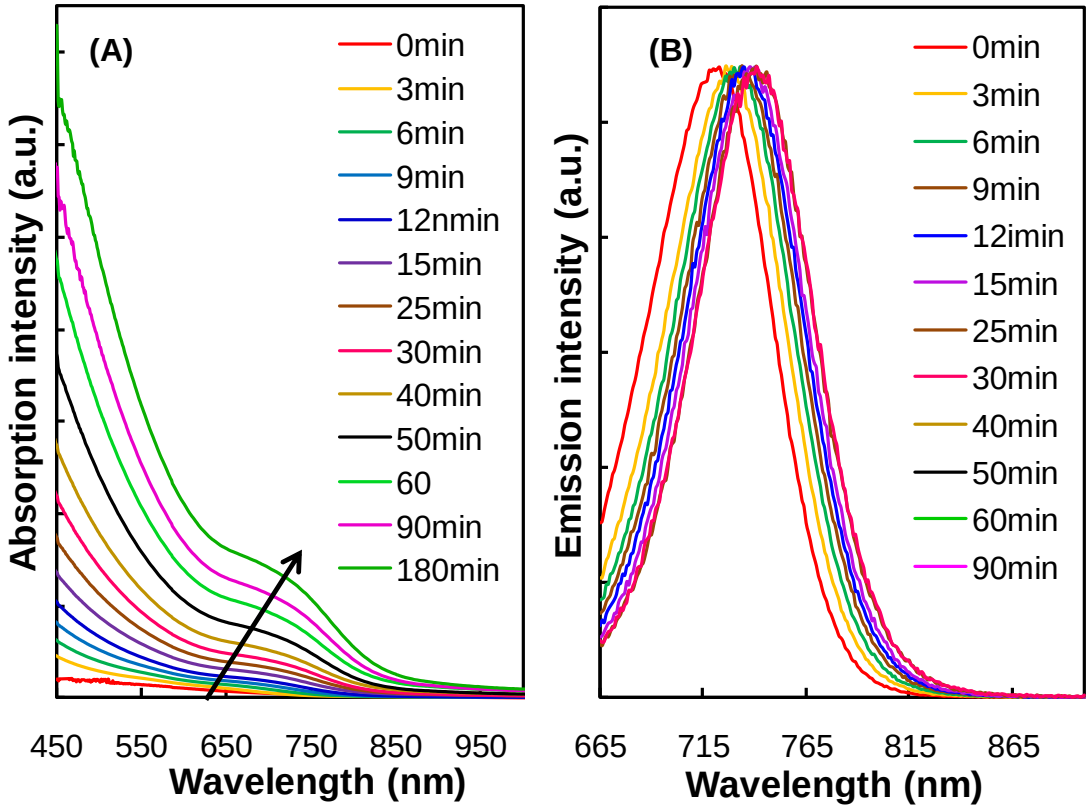

Figure 4.1 Characterization of samples synthesized at 50ºC, molar ratio between oleic acid, PbO and $(TMS)_2S$=5:2:1. (A): absorption spectra; (B): corresponding emission spectra at first exciton wavelength

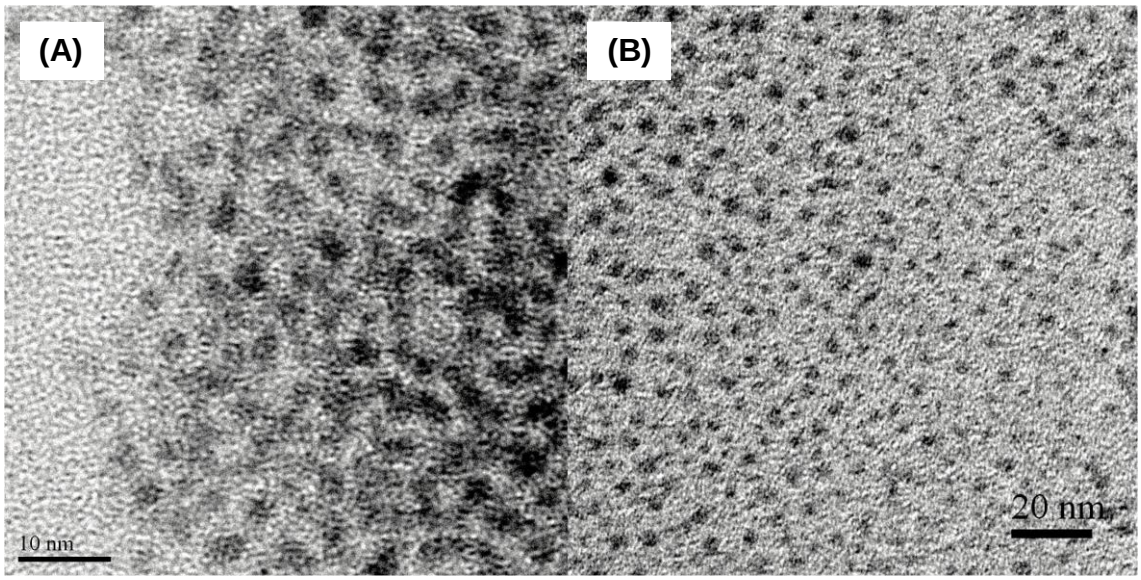

Figure 4.2 TEM images of PbS QDs synthesized at 70°C, oleic acid: PbO:$(TMS)_2S$ molar ratio=5:2:1, sample taken at 45 minutes after reaction commencement

To understand the impacts of different aspects in the reaction, three independent reaction parameters were controlled. PbS QDs were synthesized under different temperatures from a room temperature (24ºC) up to 120ºC, and the molar ratio of stabilizer oleic acid to lead oxide were varied from 5:2 to 10:2 (Table 4.1). For each temperature and stabilizer-Pb ratio, samples were taken at different time intervals during the reaction to monitor particle growth.

Table 4.1 Designed experiments that were carried out at different reaction parameters. The columns represent different temperatures as listed above, the rows are different feed ratios between oleic acid and PbO. The dark shade indicate experiments that were characterized by UV-Vis spectrophotometer and photoluminescence spectrometer; light grey shaded squares indicate experiments that were only characterized by UV-Vis spectrophotometer

Feed ratio \ T	24°C	40°C	50°C	60°C	70°C	80°C	90°C	100°	110°C	120°C
3:2										
5:2										
7:2										
10:2										

4.2 Nucleation

The effect of reaction time on particle growth was studied under a series of reaction conditions. At given reaction conditions, increasing reaction time always results in the increase of the first absorption peak wavelength, which is the indication of continuous particle growth. Nucleation process was studied by taking the first sample of each batch of reaction immediately after injecting sulphur precursor. Rapid change of solution colour from colourless to dark brown was observed for all samples within several seconds, indicating rapid nucleation rates.

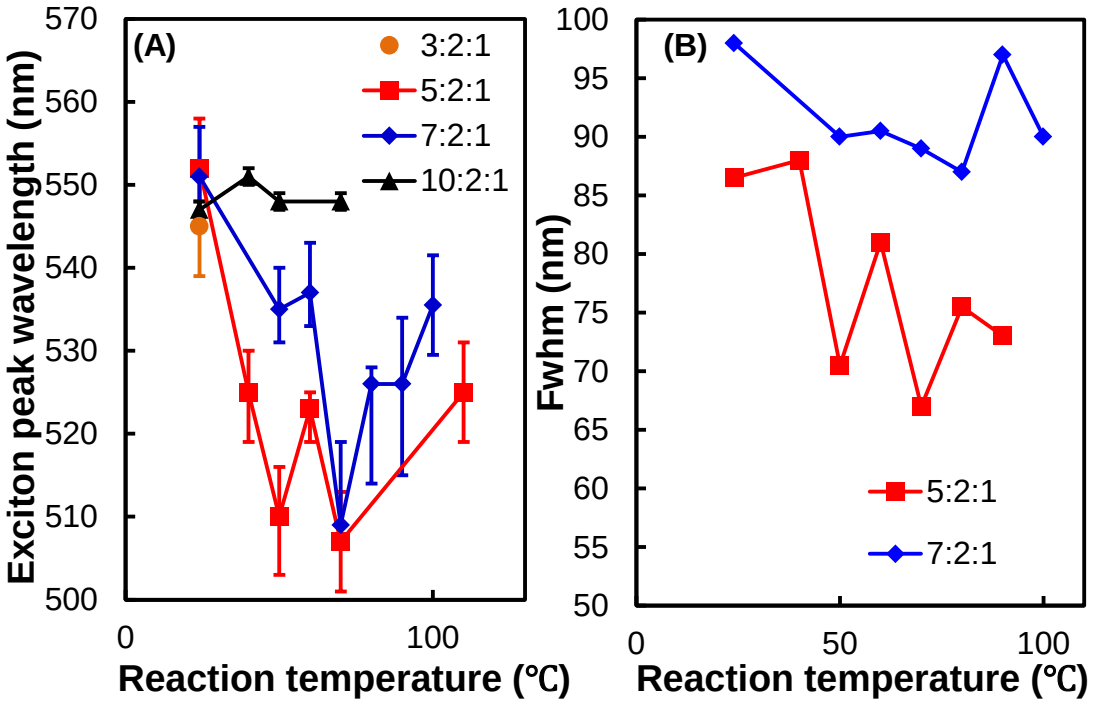

Figure 4.3 Effect of reaction temperature and oleic acid feed on initial nucleation. A: first exciton wavelength for the nucleation samples synthesized under temperature from 24ºC to 110ºC and oleic acid: PbO: $(TMS)_2S$ molar ratio from 3:2:1 to 10:2:1; B: FWHM of photoluminescence spectra under different temperatures at the oleic acid: PbO: $(TMS)_2S$ feeds of 5:2:1 and 7:2:1

Figure 4.3 compares the first exciton wavelength and FWHM of emission spectra of nucleation samples taken from different reaction batches to understand the effect of temperature and stabilizer concentration. The first exciton wavelengths in Figure 4.3 A were taken as the wavelength value of the first peak in every absorption spectrum. For the spectra that do not have sharp absorption peaks (i.e., spectra of 0 minute to 3 minutes samples in Figure 4.1 A), the first order derivatives were taken and the wavelengths with minimum slope were used. The FWHM data in Figure 4.3 B were calculated as the full-width at half intensity peak value of corresponding emission spectra. In Figure 4.3 A, the first exciton wavelengths vary in a range from 507 to 552 nm. By increasing the oleic acid: PbO feed from 5:2 to 10:2, the exciton peak wavelengths show an increasing trend at constant temperature (as shown in Figure 4.3 A). On the other hand, by increasing feed ratio from 5:2 to 7:2, the FWHM of the photoluminescence spectra also increases. There is a hint of increasing in nucleation size, and size randomness with increasing oleic acid feed. Although one would assume that the increase in stabilizer amount should make it easier for small crystallite to be captured, resulting in larger number of smaller nucleation, the data indicates that the average size of initial nucleation actually increases with stabilizer feed. Similar situation has been observed for CdSe QDs with oleic acid as ligand as well, though no clear explanation was given.[56]

In Figure 4.3 A, the first exciton wavelength decreases from 552 nm at room temperature to 525 nm at 110ºC with feed ratio 5:2:1, and from 551 nm at room temperature to 535 nm at 90ºC with feed ratio 7:2:1. This could be possibly indicating the decrease in nucleation

size with increasing temperature. It should be mentioned that due to the small size of the initial samples, the first exciton wavelengths were taken from maximum in first order derivative. Error may be introduced by using such a calculation method, and the random error in individual experiments may also compromise the data accuracy. Nonetheless, this reduction in initial sample size with temperature could be explained by the kinetic increase of precursor activity, resulting in larger number of smaller nucleation. The relatively uniform nucleation size distribution comparing to large difference in stabilized particle sizes (Figure 4.3A) observed for the reactions at various conditions may imply a critical nucleation size r*.

The critical size r* could be roughly estimated by Scherrer formula[81]:

$$\varepsilon = \frac{\lambda}{b\cos\theta} \tag{3}$$

where ε is the apparent crystal size, λ is the wavelength of the radiation, b is the additional broadening and θ is the Bragg angle. For the 'true' size of the particle, which is the cube root of the crystallite volume, it is given by

$$p = \frac{4}{3}\pi r^3 = K \cdot \varepsilon \tag{4}$$

where K is the Scherrer constant. The Scherrer constant is dependent on the definition of 'breadth', the crystal shape and crystallite size distribution. The spherical crystallite shape was assumed, and K and θ were adopted from another reference.[82] The critical particle size

was calculated to be $r^*=2.2\pm0.1$ nm in diameter. It should be noticed that these calculated size were only for the understanding of size change under different reaction parameters and does not necessarily represent the true size value. For more accurate size calculation, especially for particles with diameter smaller than 3 nm, a model on atomic level could be built. A valuable example of PbS nanoparticles atomistic model and related calculation of atom numbers, particle size and surface ligand coverage were given by E.H Sargent's group very recently.[78]

Figure 4.3 B shows the increase in FWHM with oleic acid feed, corresponding to the increase in particle size distribution. The increase in FWHM with increasing stabilizer feed is understandable, because increased free ligand would more easily encapsulate the crystallite cluster and resulting less uniformity in size. It should be mentioned here that due to the measuring limitation of the spectrofluorometer, only two sets of data were used in this figure.

4.3 Particle growth and saturation

After rapid nucleation, particles were observed to go through a stage of particle growth before reaching the saturation stage where particle size reaches constant. The reaction parameters were observed to have effect on size increasing rates, final particle sizes and size dispersity of the particles. These parameters are discussed separately.

4.3.1 Time dependency

Figure 4.4 illustrates the time dependency of first exciton wavelength under different reaction temperatures from room temperature up to 120ºC, with oleic acid to PbO molar ratios controlled at 5:2 (A), 7:2 (B) and 10:2 (C). It could be observed that all first exciton wavelengths show rapid increase at the initiate stage of the reaction. The fast rate of particle growth is corresponding to the rapid colour change from colourless to dark brown observed during reaction. The increase rate of first exciton wavelength (represented by the slope of the curve) gradually decreases as reaction time prolong, until reaching zero. This is because as the precursors were gradually consumed, the lowered concentration of precursors would reduce the reaction rate, until none dissolved precursors were present in the solution and the particles reached constant size. The particle growth was also studied at different temperatures, from room temperature (24ºC) to 120ºC. As shown in Figure 4.4, by increasing reaction temperature, the initial slopes of the curves become steeper, correlating to faster growth of particle size and shorter time used to reach maximum

wavelength. The results are partly in agreement with previous study which showed the increase of particle size with reaction time and temperature,[66,67] but no significant particle growth after 'size-focusing' stage was observed, even when the reaction time was prolonged to 200 minutes (Figure 4.4 A).[67] Such observation could be easily understood, because increasing reaction temperature would significantly increase the reactivity of the precursors, making the increase in curve slope a reasonable outcome. The relation between curve slopes in Figure 4.4 and reaction rate will be further discussed in Section 4.4.

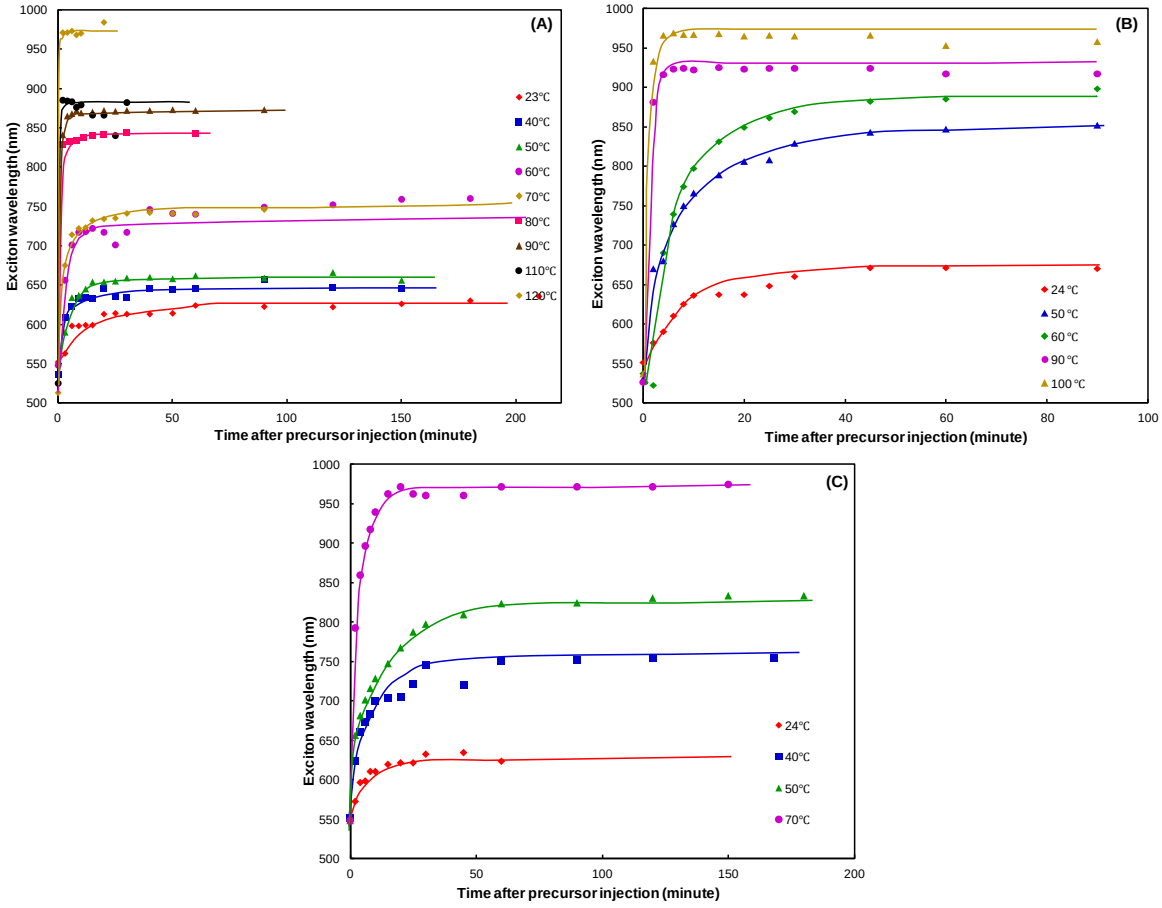

Figure 4.4 Time dependency of first exciton wavelength on the reaction temperature for PbS samples synthesized with molar ratio OA: PbO=5:2 (A), 7:2 (B) and 10:2 (C), temperature ranging from 24ºC to 120ºC

Figure 4.5 A and B show the FWHM of photoluminescence spectra taken at different temperatures with fixed oleic acid: PbO: $(TMS)_2S$ molar ratio of 5:2:1 and 7:2:1, respectively. As seen from both figures, the first sample which was taken immediately after precursor injection in each temperature reaction shows larger FWHM comparing to the samples taken later. As reaction time increases, the FWHM value shows narrower distribution, and it is found that after reacting for 6 minutes, FWHMs of the taken samples are generally narrowed down to 65-70 nm, indicating a narrower size distribution. No obvious effect of temperature on FWHM was observed. This is because the process of particle growth is generally believed to be Ostwald ripening,[57] and the effect of small changes in temperature will be obscured by the effect of time. The calculated average FWHM for samples taken after reacting for 10 minutes is 67.8 ± 5.2 nm for all measured samples. Such a value is comparable to the best reported FWHM for PbS QDs.[66,83] Therefore the fabricated particles are of good size monodispersity. It should be mentioned that during the washing process after QD synthesis, all supernatants were colourless or almost colourless, and size selection during washing stage where small-sized particles remain in supernatant was not dominantly responsible for the narrow size dispersion. It should be noticed that due to the limitation of measuring wavelength for the spectrofluorometer, FWHM data from reactions with elevated temperature and oleic acid feed were not available. The results show that in order to obtain high quality QDs, it is crucial to ensure that reaction time is long enough for particles to reach good monodispersity. From experimental data, obtaining samples after 10 minutes of reaction is adequate for most synthesis conditions.

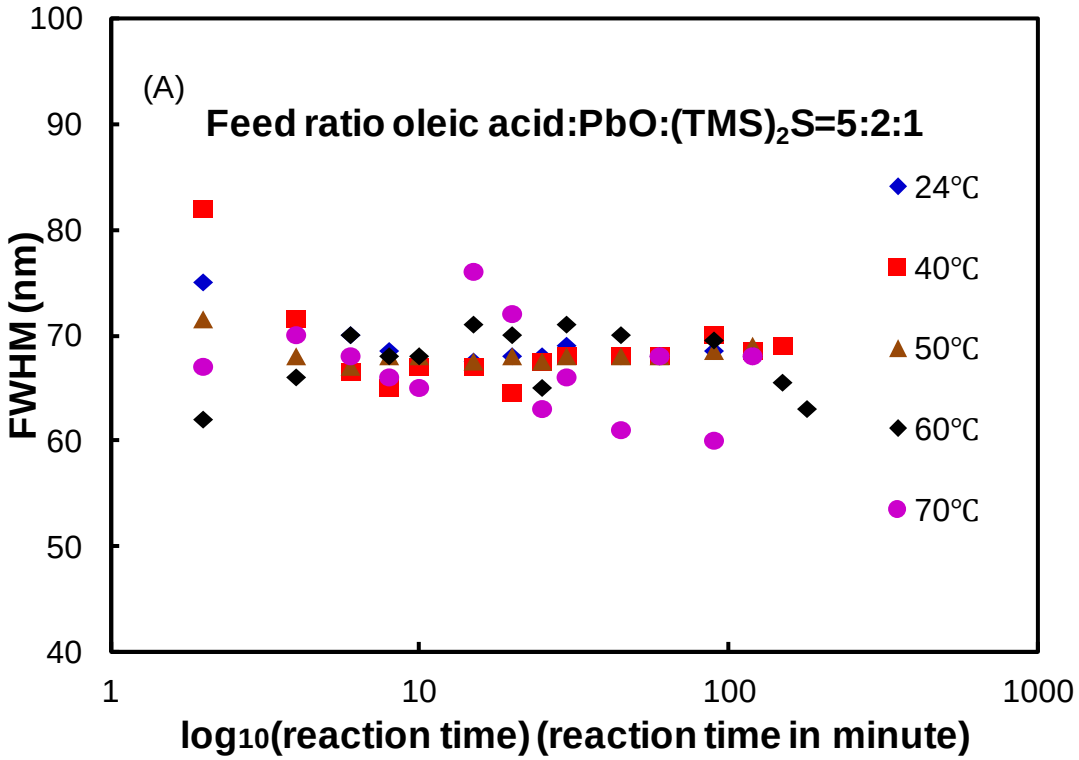

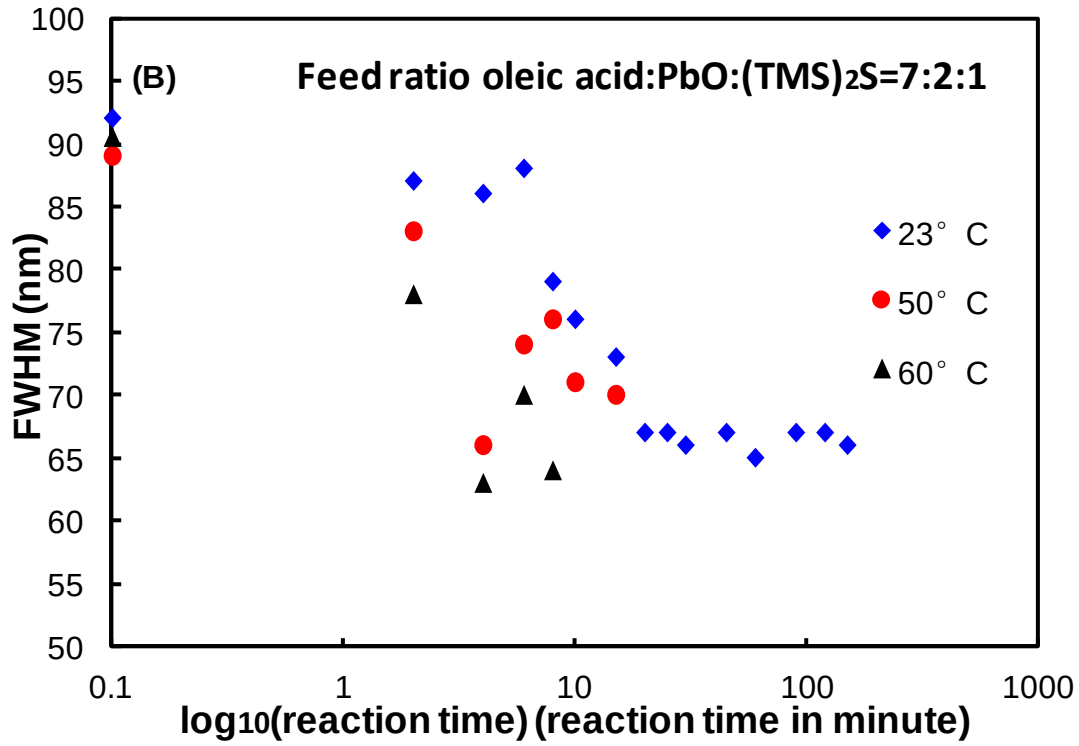

Figure 4.5 FWHM of emission spectra of samples taken at different reaction time and temperatures. The feed ratio oleic acid: PbO:$(TMS)_2S$ is 5:2:1 in (A) and 7:2:1 in (B)

4.3.2 Reaction temperature

One of the most evident effects of increasing reaction temperature on PbS QD synthesis is the increase of particle size. From Figure 4.4 it could be seen that for every reactant ratio controlled, increasing temperature could always results in an increase in the exciton wavelength. It could be observed that the initial slope for the curves increase with temperature, and by doubling the reaction temperature, the time required reaching a constant particle size more than halves. This indicates that the temperature has a major impact on particle size and the size increase rate. These data will be further discussed in Section 4.4.

The ‘saturated’ particle size is plotted against temperature to understand their relation. Figure 4.6 shows the average exciton wavelength of size-saturated particles against reaction temperature. For each curve in Figure 4.6, the average exciton wavelength for size-saturated particles was obtained by calculating the average wavelength for every data after the logarithm growth stage (please refer to Section 4.4 and Figure 4.9 for the determination of logarithm stage for each curve). For different ratios between oleic acid and PbO, the increasing tendency appears to be different. When the molar ratio of oleic acid: PbO is 5:2, the wavelength-temperature curve appears binominal; when the ratios increase to 7:2 and 10:2, the increasing tendency appears more linear. As the synthesis under the ratio of 3:2 was proven insufficient for particle growth, we weren’t able to draw a similar curve of exciton wavelength to temperature. Limited theory was available to

explain the difference in trends under different ratios; but the figure does indicate the possibility that the relation between average exciton wavelength and temperature might be different for higher and lower oleic acid concentrations.

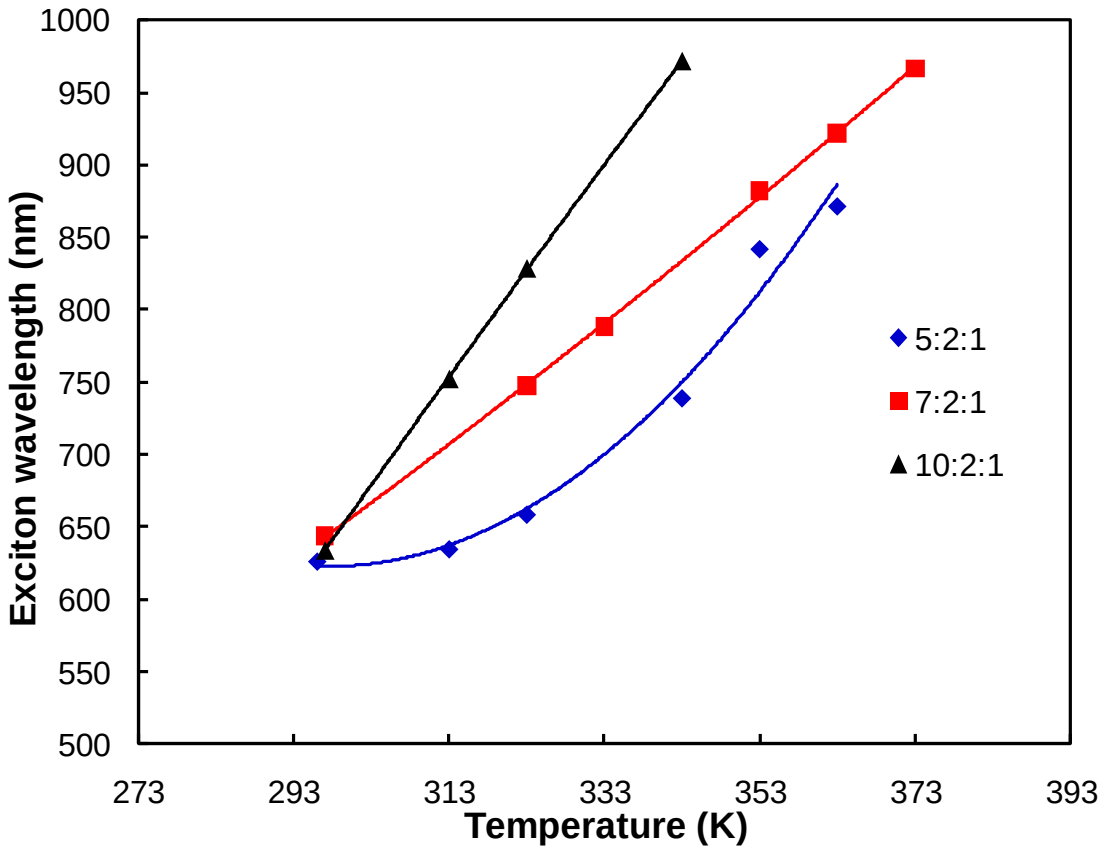

Figure 4.6 Relation between first exciton wavelength of size-focused PbS QDs and reaction temperature. Different molar ratios between oleic acid, PbO and $(TMS)_2S$ are compared, as indicated in figure legends

4.3.3 The Reactant Ratio

For the synthesis of PbS QDs, the feed ratio between PbO, the sulphur precursor $(TMS)_2S$ and the ligand oleic acid plays a key role in determining particle size. Previous study [66] has reported that by increasing the molar ratio between PbO and $(TMS)_2S$ from 2:1 to 4:1, the absorption peak wavelength showed slight blue-shift at temperature above 70ºC, corresponding to size decrease of a few angstroms. When the PbO feed is too small (1:1 molar ratio to $(TMS)_2S$), the particle growth is too fast to observe well-defined absorption peak and emission, but when the molar ratio was increased to 8:1, the absorption peak showed significant increase. A controllable system was chosen to study the change of exciton wavelength and the ratio of 2:1 between PbO and $(TMS)_2S$ was fixed. It is also found that excessively small concentration lead to extended reaction time to reach desired particle size, so the concentration of PbO and $(TMS)_2S$ was controlled at 0.067 mol/L and 0.033 mol/L, respectively. To study the effect of reactant feed on particle growth, the concentration of oleic acid was controlled. Four different molar ratios between oleic acid and PbO were investigated, namely 3:2, 5:2, 7:2 and 10:2, corresponding to oleic acid concentration of 0.100 mol/L, 0.167 mol/L, 0.233 mol/L and 0.333 mol/L.

Particle growth for oleic acid and PbO feed of 3:2 at room temperature was studied to understand the nucleation and particle growth at low ligand feed. Room temperature was chosen for the reaction so that with reduced reactivity, the particle growth behaviour could be better observed. Figure 4.7 shows the change of first exciton wavelength with reaction

time (A) and the first order derivative plots of the absorption spectra at 20 minutes and 180 minutes after precursor injection (B). With increasing reaction time, it is observed that after 20 minutes of reaction, two peaks appear in the derivative plot, corresponding to two absorption peaks at 515 nm and 552 nm (Figure 4.7 A). As reaction time prolongs, both absorption peaks are observed for the taken samples with relatively constant peak wavelength (Figure 4.7 A), though it could be observed with Figure 4.7 B that the slope at around 515 nm decreases while the slope at around 552 nm increases. Due to the similarity in wavelength between both peaks, only one peak in emission spectra is observed. However it is noticed that the FWHM of the spectra are significantly larger than the average value of 68.6 nm (Figure 4.5). The inset in Figure 4.7 B shows the emission spectrum of sample taken at 180 minutes after injection, with FWHM of 89.0 nm.

Figure 4.7 shows that two absorption peaks exist after 20 minutes reaction and the peaks do not merge into a single peak with prolonged reaction time. This interesting observation could be explained by the oleic acid feed. Due to the low oleic acid feed, the amount of precursors for particle growth is limited. Therefore after rapid nucleation, a large population of nuclei is formed, most of the ‘free’ precursors in the solution are soon consumed and smaller particles start to dissolve for larger particle growth. This is in support of the general belief that Ostwald ripening is the dominant mechanism for PbS and Cd chalcogenide QD growth, where small particles break down to promote the growth of larger particles. But no similar behaviour is observed for reactions at higher oleic acid feed, two possible reasons might be responsible for this. First, by increasing the concentration of

Pb precursor, the particle growth would be more dependent on the free precursor than Ostwald ripening; secondly, the reaction rate will be much increased with higher precursor concentrations and reaction temperatures, making it more difficult to observe similar phenomena even if they occur.

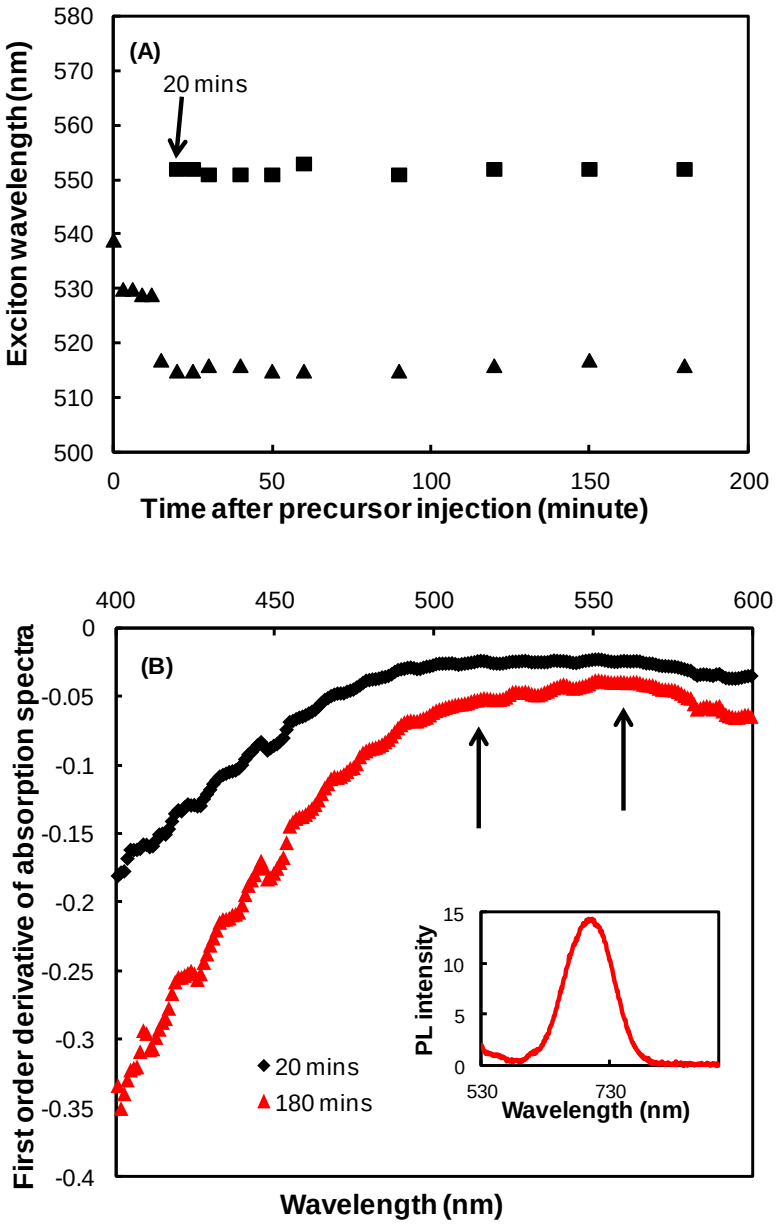

Figure 4.7 Time dependency of first exciton wavelength (A) and the first order derivative of the absorption spectra at 20 minutes (black curve) and 180 minutes (red curve) after precursor injection (B). Oleic acid: PbO feed=3:2, reaction temperature at 23.5ºC. Inset shows the emission spectrum of sample taken at 180 minutes

The effect of stabilizer feed on FWHM is also studied. Figure 4.8 shows the photoluminescence spectra FWHM of samples taken at different time. Both samples were reacted at room temperature (24ºC for Figure 4.8 A, 40ºC for Figure 4.8 B) where the triangle data series are for double oleic acid feed and normal feed is shown in square series. Slight increase in FWHM could be observed for samples with a higher oleic acid feed taken within a few minutes, but after reacting for 10 minutes for 24ºC and 6 minutes for 40ºC all samples showed compatible particle size distribution. This also proves that the increase in stabilizer concentration could make it easier for small crystal clusters to be captured, resulting in broader size distribution. However, from the final size distribution after 10 minutes reaction (Figure 4.4), it could be seen that for the range of parameters controlled, the final particle size distribution is relatively constant.

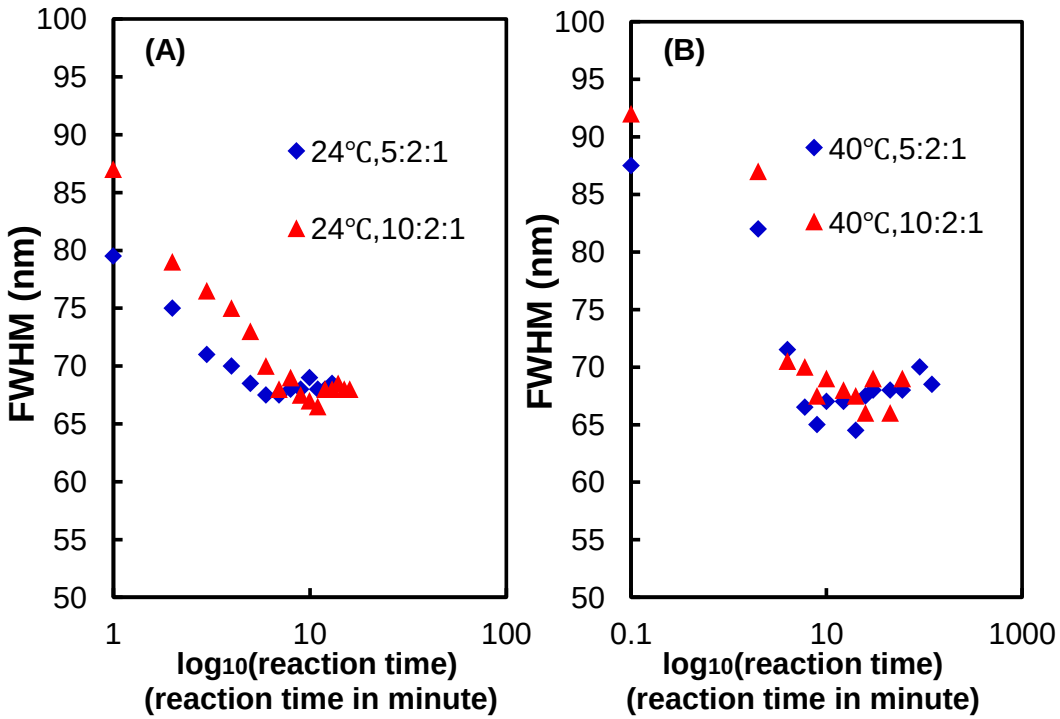

Figure 4.8 FWHM of photoluminescence spectra for samples synthesized at 24ºC (A) and 40ºC (B), with different oleic acid: PbO: $(TMS)_2S$ molar ratio as listed in legends

4.4 Understanding of particle growth

The particle growth for PbS QDs is generally believed to be Ostwald ripening, in which case small particles dissolve and realign on (111) facet of larger particles. Since the exciton wavelength is corresponding to the band gap of the nanoparticles, which is in turn dependent on particle size, the rate of crystal growth could be represented by the slope of exciton wavelength to reaction time. It is noticed that for the crystal growth stage (before the saturated particle size is reached), the exciton wavelength vs. reaction time curves follow a logarithm form. It should be mentioned that the exciton wavelength plot was used for further calculation of reaction rate instead of the particle size. This is not only because the wavelength data could be easily converted to particle band gap, but also because in practical synthesis procedure, it is more intuitive and practical to control the exciton wavelength of particles instead of actual particle size. Figure 4.9 shows the natural logarithm fitting for the exciton wavelength to reaction time curves at the reaction temperature ranging from room temperature to 90ºC and molar ratio between oleic acid and PbO from 5:2 to 10:2. The fitting equations and R^2 are listed in Table 4.2.

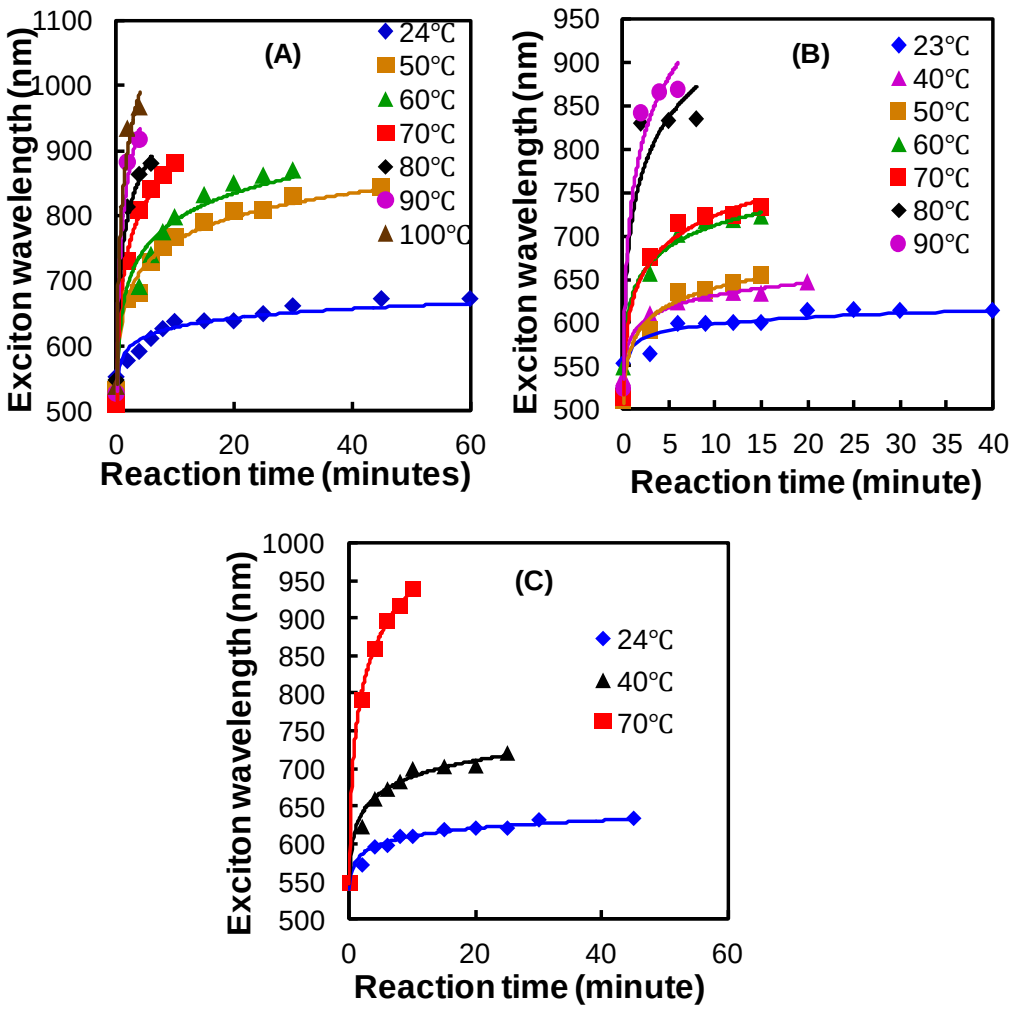

Figure 4.9 Natural logarithm fitting for first exciton wavelength-reaction time curves at particle growth stage. (A): molar ratio between oleic acid, PbO and $(TMS)_2S$ is 5:2:1; (B): molar oleic acid: PbO: $(TMS)_2S$=7:2:1; (C): molar oleic acid: PbO: $(TMS)_2S$=10:2:1

Table 4.2 Natural based logarithm fitting equations and R^2 for exciton wavelength-time curves

T (℃)	Oleic acid: PbO: $(TMS)_2S$ 5:2:1		Oleic acid: PbO: $(TMS)_2S$ 7:2:1		Oleic acid: PbO: $(TMS)_2S$ 10:2:1	
	Fitted equation	R^2	Fitted equation	R^2	Fitted equation	R^2
24	y = 11.37ln(x) + 571.87	0.9179	y = 19.60ln(x) + 582.04	0.9204	y =15.10ln(x) + 575.14	0.9555
40	y = 20.37ln(x) + 584.35	0.9915	N/A		y =31.12ln(x) + 617.24	0.9794
50	y = 28.86ln(x) + 573.30	0.9783	y = 53.03ln(x) + 638.88	0.9812	N/A	
60	y = 36.03ln(x) + 629.09	0.9862	y = 59.11ln(x) + 655.25	0.9624	N/A	
70	y = 44.78ln(x) + 620.29	0.9886	y = 80.94ln(x) + 690.72	0.9959	y =84.85ln(x) + 741.01	0.9992
80	y = 84.59ln(x) + 728.17	0.9535	y = 83.53ln(x) + 741.99	0.9953	N/A	
90	y = 89.06ln(x) + 739.45	0.9683	y =109.55ln(x) + 782.48	0.9907	N/A	

R^2 above 0.95 is observed for most of the fitting equations. Considering experimental error between different synthesis batches and data noise, the R^2 values indicate good agreement between experimental data and fitted equation. It is noticed that for samples reacted at room temperature the R^2 is exceptionally low. This could be explained by the effect of low reaction temperature. Lower reaction temperature would result in lower kinetic movement, and thus reducing the homogeneity of crystallite size in reaction solution, which would in turn leads to larger variation in obtained data. The logarithm fitting was not carried out for the reactions above 100ºC because the reaction rate was too high at such temperature. Very often the second sample taken is already very close to or reached saturated particle size.

From Table 4.2 it is easily noticed that the constant in front of the logarithm term is showing interesting pertinence to reaction temperatures. This is considered reasonable because in a general chemical reaction between reactants A and B, the reaction rate could be calculated as

$$r = k(T) \cdot [A]^{n'} \cdot [B]^{m'} \quad (5)$$

Therefore, the reaction rate should be represented by the multiplication of a temperature dependent term k(T) and a concentration, or time, dependent term. From the fitted equation

$$\lambda = \alpha \cdot \ln(\text{time}) + \beta \quad (6)$$

if we consider the first order derivative (which is the increase rate of exciton wavelength, or the increase rate of particle size) a function of reaction rate, then

$$f(r) = \alpha \frac{1}{\text{time}} = \mathbf{K(T)} \frac{F(C)}{\text{time}} \quad (7)$$

where f(r) is the function of reaction rate, **K(T)** is a temperature dependent function (capital **K** is used to differentiate from the reaction rate constant k), and F(C) is the concentration dependent function. For a given reactant ratio where the total volume is controlled constant, term α is a function of temperature. The relation between reaction temperature and the term α was further investigated.

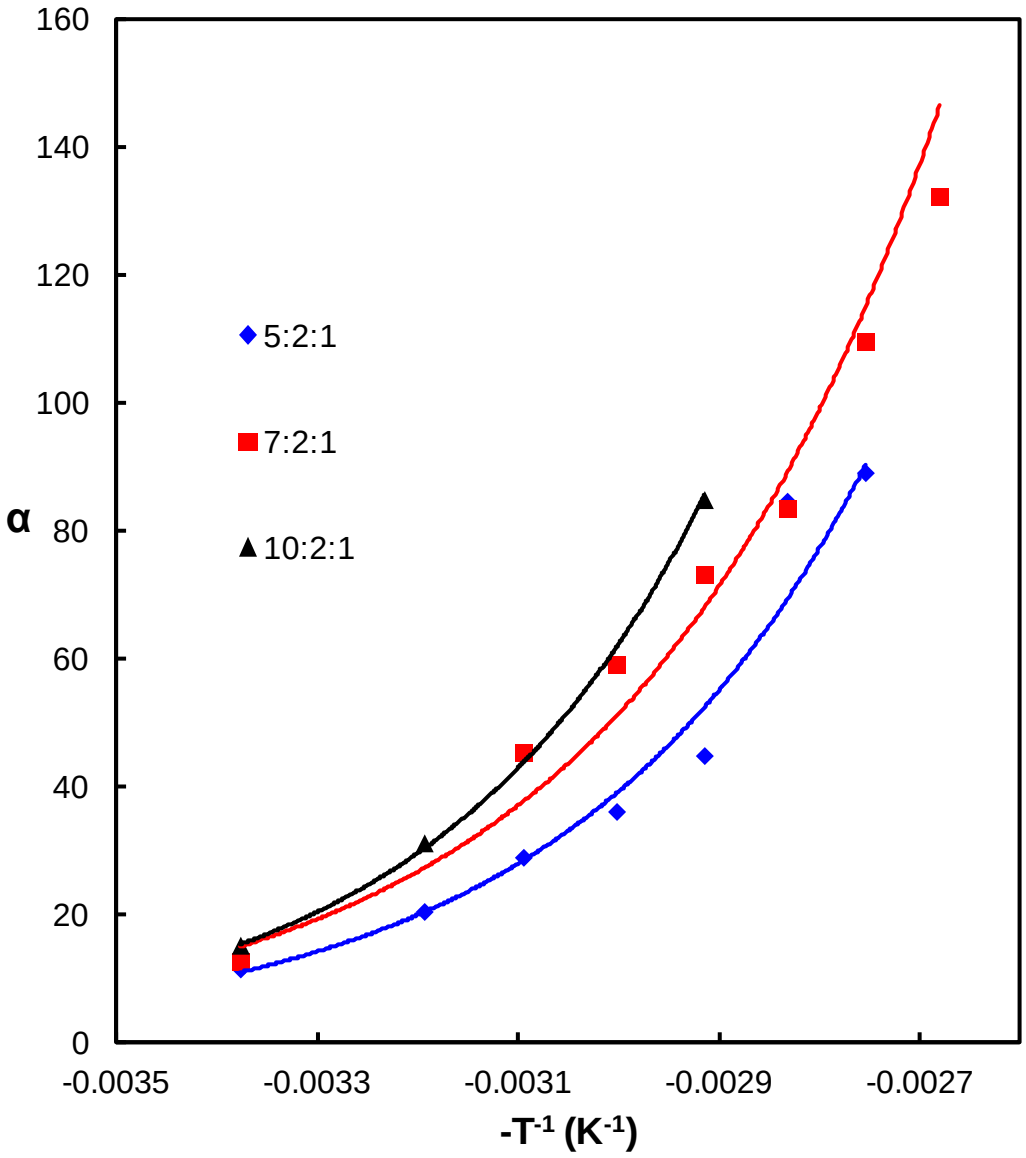

Figure 4.10 Plotted relations between the reciprocal of reaction temperature and fitted logarithm term α at different oleic acid feeds. Solid line in corresponding colour indicate plot fitted to an exponential function, inset legend indicates the different molar ratio between oleic acid, PbO and $(TMS)_2S$

Table 4.3 Fitted equations of α as an exponential function of temperature

Molar oleic acid: PbO:$(TMS)_2S$	**Fitted exponential equation**	**R^2**
5:2:1	$y = 1.00\times10^6e^{3390.3x}$	$R^2 = 0.9780$
7:2:1	$y = 0.95\times10^6e^{3275.2x}$	$R^2 = 0.9704$
10:2:1	$y = 4.00\times10^6e^{3720.6x}$	$R^2 = 0.9993$

By plotting α against reciprocal of temperature, an exponential relation is observed. Although for oleic acid: PbO: $(TMS)_2S$ molar ratio of 7:2:1, the equation is not fitted as well as the other two, a clear tendency of the curves could be observed. The reason that α is plotted against the reciprocal of temperature, apart from the observed good consistency proved by R^2 above 0.97, is that this exponential relation could effectively explain the observed temperature dependency. Reaction rate constant k(T) is calculated from Arrhenius Equation:

$$k(T) = A \cdot e^{-\frac{E_a}{RT}} \tag{8}$$

where E_a is the activation energy and R is the gas constant. If the proposed $\alpha = \mathbf{K}(\mathbf{T}) \cdot F(C)$ is correct, then we should be able to observe a relation between α and temperature similar to that of k(T) and temperature, because by controlling the reactant feed and total volume the concentration dependent term $F(C)$ should be able to consider constant. The equations shown in Table 4.3 confirm our assumption. In the fitted expression $\alpha = P \cdot e^{Q\cdot(-\frac{1}{T})}$, the power term $Q \cdot (-\frac{1}{T})$ should be corresponding to $\frac{E_a}{R} \cdot \left(-\frac{1}{T}\right)$, therefore theoretically this term should be constant for a given reaction. From the fitted equations the activation energy for Ostwald ripening of PbS QDs was calculated to be Ea=28.78$\pm$2.15 kJ/mol. This result is comparable to Ea=25.7 kJ/mol reported for ZnS nanoparticles ripening under hydrothermal conditions.[84]

4.5 Summary

The effect of reaction time, temperature and stabilizer feed is studied for PbS QD synthesis. The particle growth could be understood in three stages, the nucleation stage, the particle growth stage and the saturation stage. The nucleation stage was studied by examining the samples taken immediately after precursor injection, and nucleation size was observed to increase with decreasing temperature and increasing stabilizer feed. The particle growth stage is generally believed to be dominated by Ostwald ripening. The experiment results seem to agree with this theory. The particle growth rate and kinetics are further discussed and the activation energy for Ostwald ripening was proposed to be 28.8 kJ/mol in average. The saturated particle size is found to increase with increasing temperature and oleic acid concentration, which is in agreement with previous studies.

Chapter 5 Ligand Exchange of PbS Quantum Dots Using Tridentate Hydrophilic Polymer with Enhanced Quantum Yield

5.1 General approach of atomic-ligand exchange

Before applying the PbS QDs of selected size in organic PV devices, surface ligand modification via ligand exchange is necessary for successful combination with conducting polymers. To examine the effect of different ligand exchange methods on optical properties, modified poly(ethylene glycol) methyl ether (mPEG) was chosen as the model ligand to transfer synthesized PbS QDs into polar solvents. This new ligand is chosen with a large difference in chemical and physical properties from the oleic acid, we could investigate the reaction conditions and change in optical properties of the particles in an extreme condition.

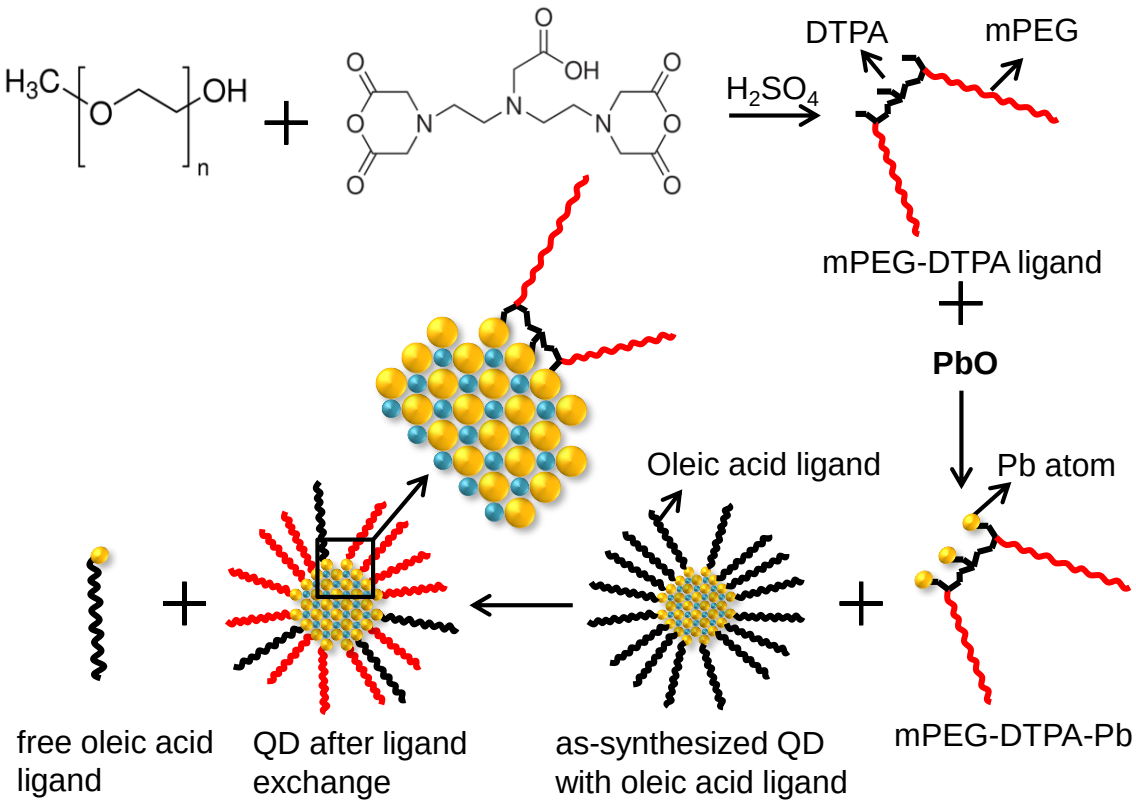

Figure 5.1 Scheme for the 'atomic-ligand' approach used for PbS QDs

The approach used for hydrophilic ligand exchange in this chapter is depicted in Figure 5.1. MPEG (molecular weight Mn=5000) was modified with diethylenetriaminepentaacetic dianhydride (DTPA anhydride) to form a tri-dentate molecule with two hydrophilic tails. The three carboxyl groups would ensure effective capture of PbS QDs while the mPEG 'tails' would ensure good dispersity in polar solvents. PbO was then reacted with the decorated mPEG ligand to form Pb-ligand units. By injecting as-synthesized PbS QDs into Pb-ligand solution the oleate ligand was exchanged with the tri-dentate mPEG ligand. The choice of experimental conditions for such approach will be given in detail in Sections 5.2 and 5.3.

5.2 MPEG modification

For the carboxyl tri-dentate modification of mPEG, dichloromethane and tetrahydrofuran (THF) were compared as solvents. Both could readily dissolve DTPA dianhydride. mPEG could be dissolved at elevated temperature, in 40ºC dichloromethane or 50ºC THF. Considering the low boiling point of both solvents, water bath was used to heat the solution. After reaction, the product was precipitated in diethyl ether and dried in vacuum. The dried product which was light yellowish in colour could redissolve in THF at 50ºC, but in dichloromethane it became insoluble at elevated temperature. Considering the higher boiling point and better solubility in THF, it was chosen as the used solvent for mPEG modification and purification.

The connection of DTPA on mPEG was characterized by titration. Figure 5.2 shows the titration plot of modified mPEG after precipitation three times. The titration was carried out using 100 mL mPEG-DTPA solution in H_2O at 17.0 g/L. The pH value of the prepared solution was measured to be 3.75. An amount of 0.01 M hydrochloric acid solution was then added drop-wise into the sample solution to adjust the pH value to 3.12. A 20 µL of 10^{-2} M NaOH solution (containing 0.2 µmol NaOH) was then drop added into the solution until pH value reached 9.50 and the conductivity and pH values were measured. The obtained data are as shown in Figure 5.2. From conductivity curve, the carboxyl group amount in solution was calculated to be 205.0 µmol, corresponding to carboxyl group concentration of 0.12 µmol carboxyl groups per 1 mg mPEG sample. The obtained product

would have the molecular weight of 10375, and the reaction yield could be calculated to be 83%.

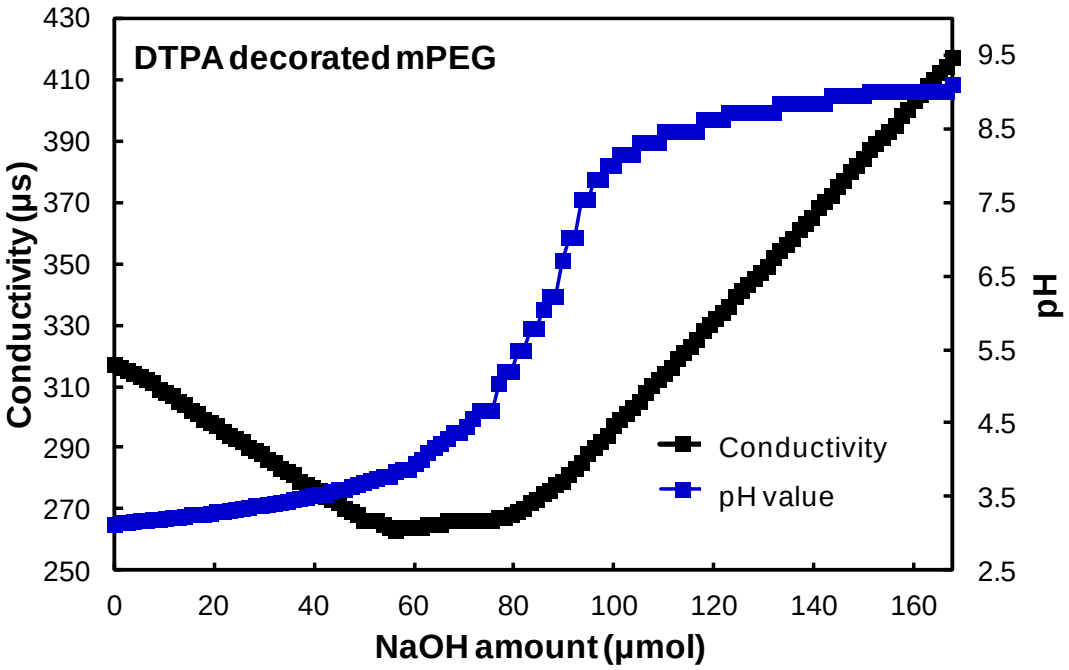

Figure 5.2 Titration plot of tri-dentate mPEG obtained after reaction with DTPA dianhydride, precipitated and dried three times; middle: tri-dentate mPEG after reaction with PbO at 60ºC; bottom: tri-dentate mPEG after reaction with PbO at 120ºC

The structural modification of mPEG was confirmed via ^{1}H NMR spectrum. Figure 5.3 shows the ^{1}H NMR spectra of mPEG (A) and mPEG modified with DTPA (B). Chemical shift at 2.959 and 2.884 ppm (peaks c and d) are corresponding to protons on DTPA structure, confirming the connection of DTPA onto mPEG. From the inset in Figure 5.3 B it could be observed that the peak area ratio between a, c and d are approximately 3:2:2, which is corresponding to the ratio between proton numbers of peaks. Due to the proton exchange, carboxyl group peaks were not observed in the NMR spectra.

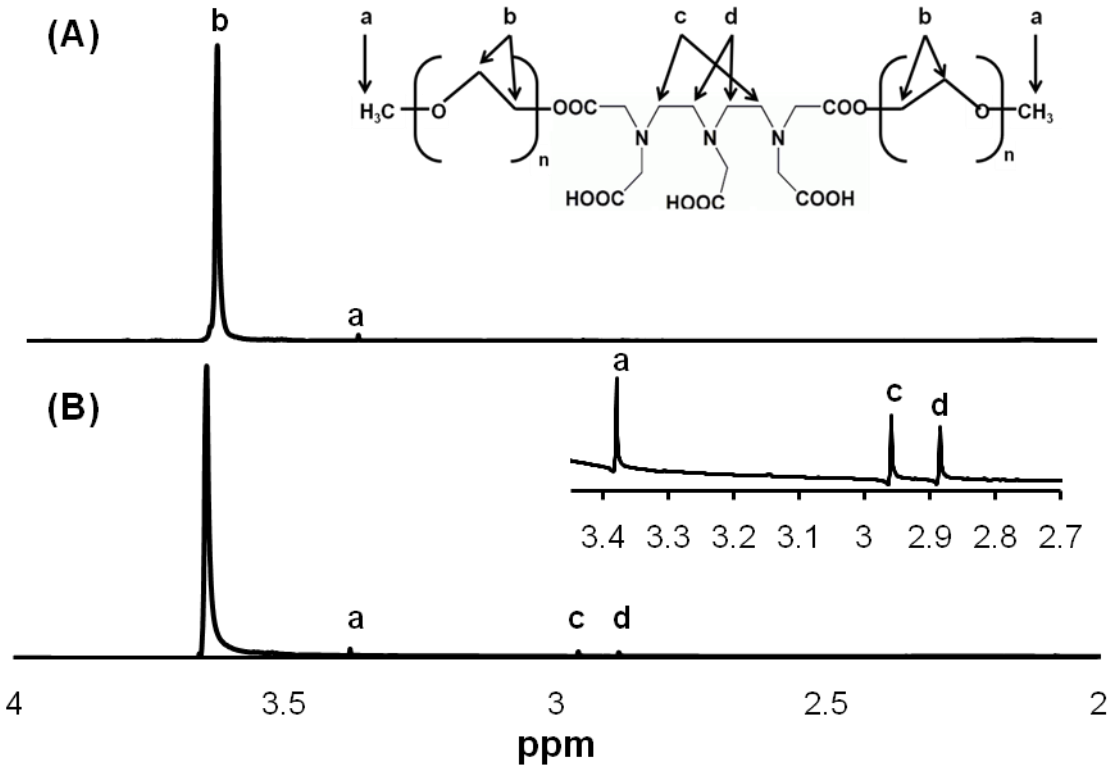

Figure 5.3 ^{1}H NMR for (A) mPEG and (B) mPEG-DTPA in DMSO-$d_{6.}$ Inset in (A) shows the molecular structure of the modified mPEG-DTPA and the inset in (B) gives the enlarged section of NMR spectrum.

5.3 Lead attachment on mPEG-DTPA ligand

In theory, the reaction between PbO and mPEG-DTPA should be similar to the PbO-oleic acid reaction for QD synthesis. Successful attachment of Pb atom on mPEG-DTPA should require good solubility of all reactants and high reaction temperature. Therefore, the solvent used for such reaction should have high boiling temperature and reactants should have good solubility in it. The initial attempt was to use ODE, as for QD synthesis it showed good solubility for PbO and the synthesized QDs, and the particles could be easily precipitated with polar solvents. The modified PEG and mPEG were found to have very

low solubility in ODE even at elevated temperature (heated to 65ºC). DMF and DMSO were both tested as ligand exchange solvent. Both solvents could dissolve carboxyl modified mPEG and mPEG. PbO shows limited solubility in both solvents, but light yellow solution could be obtained by increasing reaction time and temperature. DMF is used as reaction solvent because the reaction could readily take place at around 100ºC, but for higher reaction temperature for the atomic-ligand method DMSO might be a good choice. Figure 5.4 shows the DMF solutions after reaction between mPEG-DTPA and PbO carried out at 50ºC and 110ºC. As could see clearly, after reaction at 50ºC the solution remained colourless, after reaction at 110ºC the solution turned yellow, the colour of which came from the yellow PbO.

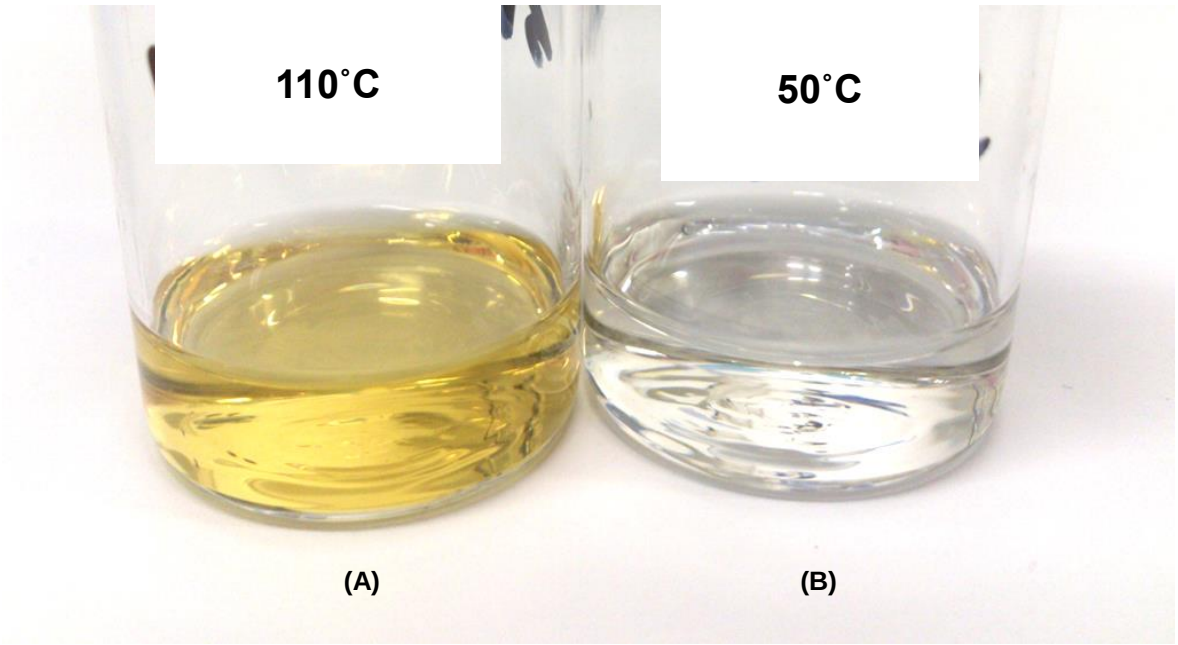

Figure 5.4 Product solutions of PbO reacted with mPEG-DTPA, in the solvent of DMF at 110ºC (A) and 50ºC (B). For both solutions samples have been centrifuged after reaction to remove any undissolved precipitated reactants and precipitated with diethyl ether twice, then redispersed in DMF to obtain clear solutions as shown

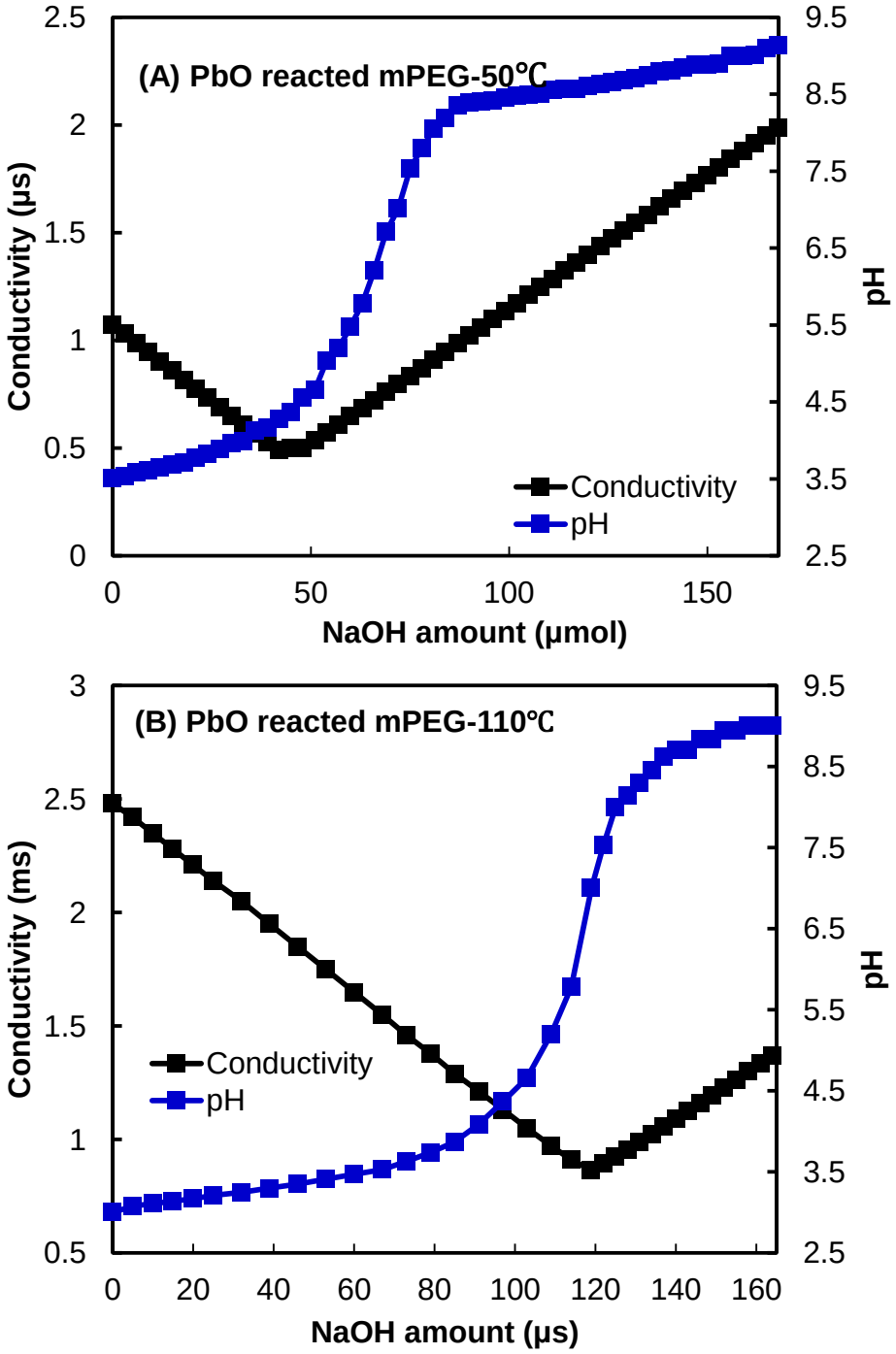

Figure 5.5 Titration plots of reaction products from PbO and mPEG-DTPA reacted in DMF at (A) 50ºC and (B) 110ºC. Both samples were centrifuged at 10000 rpm for 3 minutes. Precipitants were discarded and supernatants were precipitated with diethyl ether twice. The dried products were redispersed in H_2O and centrifuged again to obtain transparent solutions for titration

The successful formation of Pb-mPEG units was confirmed by titration. Figure 5.5 shows the titration plots for samples reacted at 110ºC and 50ºC. The preparations of titration samples and data calculation were similar to that in Section 5.2. For the reaction at 110ºC no carboxyl group was found from the titration curve (Figure 5.5 A), while for the reaction at 50ºC the carboxyl group concentration was calculated to be 0.07 μmol per 1 mg sample. Assuming that for the formed product every Pb atom is bonded with two carboxyl groups, such results are corresponding to conversion rate of around 40% at 50ºC and near 100% at 110ºC.

5.4 Comparison between atomic-ligand exchange and conventional ligand exchange

PbS QDs were exchanged with tri-dentate mPEG ligand via conventional method and atomic-ligand exchange method to compare the optical properties of the exchanged particles. For conventional method of ligand exchange, the modified mPEG-DTPA ligand was dissolved in DMF and the PbS QDs were dispersed in toluene. After adding the QD solution into the ligand solution, tiny brown droplets were soon observed within 10 minutes. After ligand exchange reaction, the aggregations could be easily transferred into H_2O solution via extraction, and no aggregation was observed in the aqua phase. Some of the particles are observed to attach on the side of the vial after reaction. For ligand exchange with atomic-ligand approach, the solution was homogeneous after QD injection.

Dark brown aggregations of QDs were observed around 25 minutes after reaction, which were also easily dissolved in ethanol or water after reaction.

Both of the dried samples from above methods are readily disperse in H_2O as well as ethanol or acetone. Figure 5.6 shows the TEM images of samples exchanged via both approaches. Figure 5.6 A shows the PbS QDs before ligand exchange. The QDs have first absorption wavelength at 605 nm and average particle size was estimated to be around 2.3 nm using method described in Section 4.2. The small particle size was chosen for the ease of further measurements and the quantum yield calculation. The as-synthesized QDs were readily dispersed in toluene and no aggregation was observed, but the particles precipitate immediately if added into solvents with higher polarity. Figure 5.6 B shows the TEM image of PbS QDs exchanged via atomic-ligand approach. Due to the high surface tension, QD-polymer agglomerations were observed in the image, and it could be seen clearly that the QDs were well dispersed inside the polymer and no aggregation was found. For the sample exchanged via conventional approach, clear H_2O solution of exchanged particles was also obtained, however a core-shell form with a PbS core in centre of the mPEG polymer is observed as shown in Figure 5.6 C. A close up image in Figure 5.6 D shows that within such core-shell structure, PbS particles still exist as individual particles instead of one large aggregation, but the PbS QDs are not as well dispersed as with atomic-ligand approach in Figure 5.6 B.

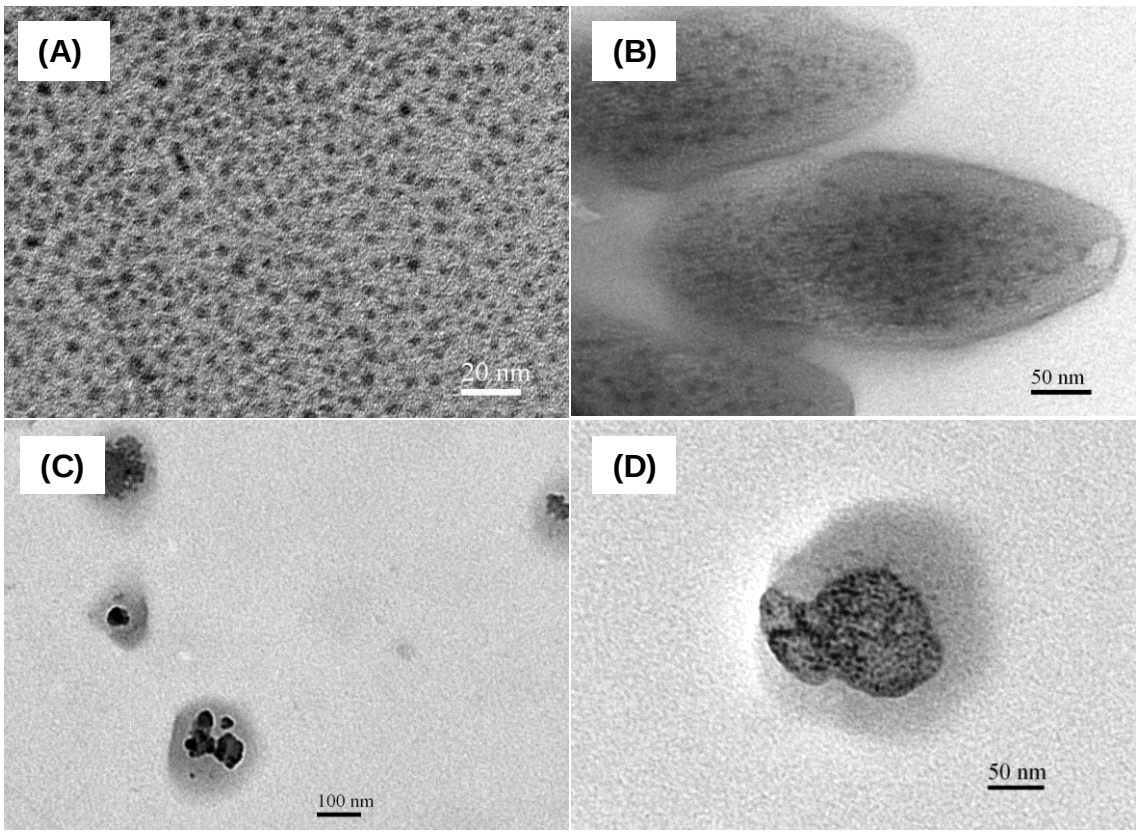

Figure 5.6 TEM images of (A): As-synthesized PbS QDs dispersed in toluene with exciton wavelength at 605 nm; (B): PbS QDs after atomic-ligand exchange with three times degas, dispersed in H_2O; (C) PbS QDs after conventional ligand exchange dispersed in H_2O; (D), the magnified image of phase-separation within a QD-polymer complex. The QDs were synthesized under oleic acid: PbO:$(TMS)_2S$ feed ratio of 5:2:1, at room temperature, reaction allowed for 20 minutes

Both precipitated samples from conventional and atomic-ligand approach were dispersed in H_2O for absorption and emission characterization, and the as-synthesized absorption spectrum is measured using the original sample solution. Figure 5.7 shows absorption spectra for as-synthesized particles, sample exchanged via conventional ligand exchange and atomic-ligand methods. For the as-synthesized particles the first exciton peak appears at 610 nm and the corresponding emission peak appears at 778 nm. It could be observed that by using atomic-ligand approach no observable blue shift was found in absorption

spectra. A red-shift of 2 nm in fluorescence peak indicates the possibility of slightly enlarging the effective particle size due to the attachment of extra Pb atoms. After conventional ligand exchange, the first absorption peak shows slight blue shift to 601 nm. The emission spectrum is less smooth comparing to that before ligand exchange, and a blue shift of 16 nm is observed after conventional exchange process, corresponding to decrease in effective crystallite size of PbS QDs. The blue shift of absorption and emission peaks after conventional ligand exchange has been reported in previous studies[85], which could be explained as the decrease in particle size caused by surface etching of the acidic ligands.

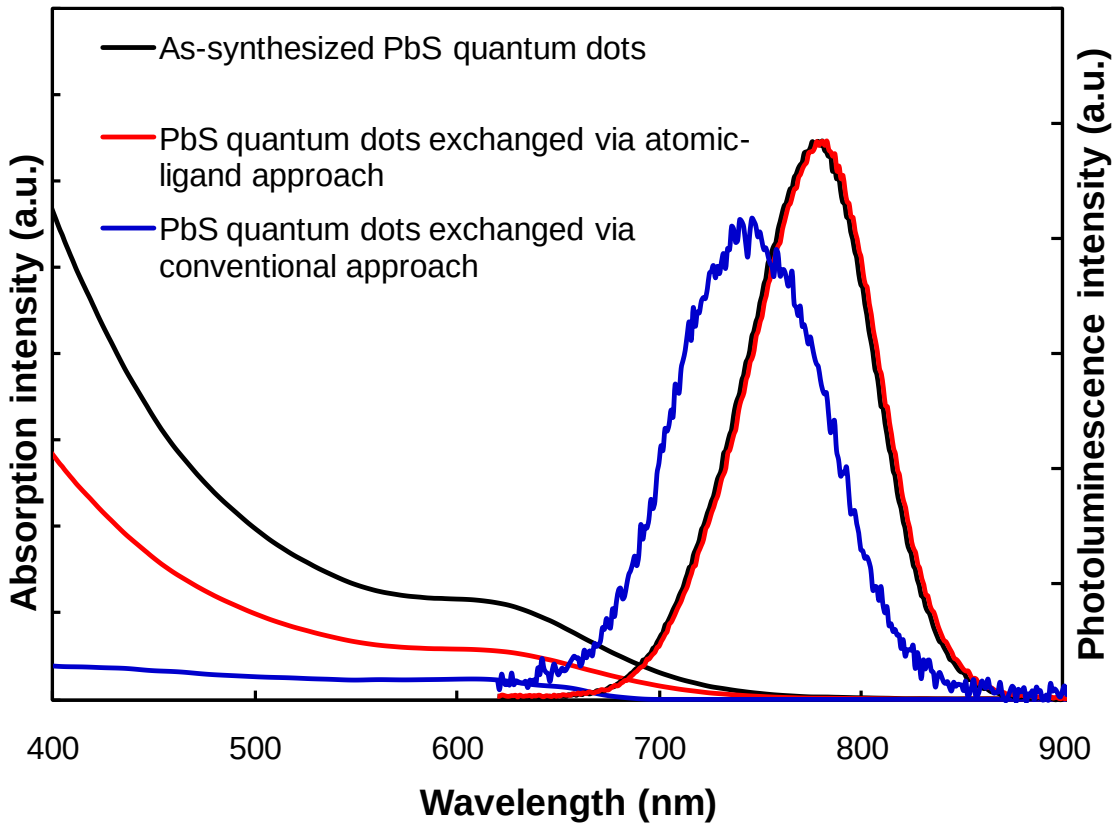

Figure 5.7 Normalized absorption and fluorescence spectra of PbS QDs before ligand exchange, after atomic-ligand exchange and conventional ligand exchange

The optical properties of PbS QDs after both ligand exchange methods were also characterized by quantum yield. Both samples after ligand exchange were stored in air under ambient temperature, and all measurements were carried out 24 hours after reaction. No particle aggregation was observed during measurement. Figure 5.8 gives the quantum yield calculation plots for each sample. Zinc phthalocyanine was used as reference dye with first absorption peak at 355 nm, the fluorescent intensity and absorption intensity of which follow linear relationship. The as-synthesized PbS QD samples used for all quantum yield measurement have exciton wavelength at 610 nm and emission peak at 778 nm. The quantum yield of as-synthesized particles (in toluene), particles exchanged via conventional method and atomic-ligand method (in H_2O) were calculated as the slope of each curve in Figure 5.8, as listed in Table 5.1. The data shows that before ligand exchange, synthesized sample has quantum yield of 87.19% in toluene, which is high comparing to previous reports.[83,86] After conventional ligand exchange process the quantum yield dramatically drops to only 2.7%. Similar drop in quantum yield after hydrophilic ligand exchange has been reported.[69,85] Such low quantum yield is understandable, as the whole ligand exchange reaction and particle precipitation was carried out in air without solvent degasification, and the pH value was not adjusted to prevent surface etching.

Using the atomic-ligand exchange process, enhanced quantum yield of 21.97% could be observed, being over 8 times that of conventionally exchanged sample. This proves that the atomic-ligand approach could effectively transfer PbS QDs into hydrophilic solvent without sacrificing too much the particle performance.

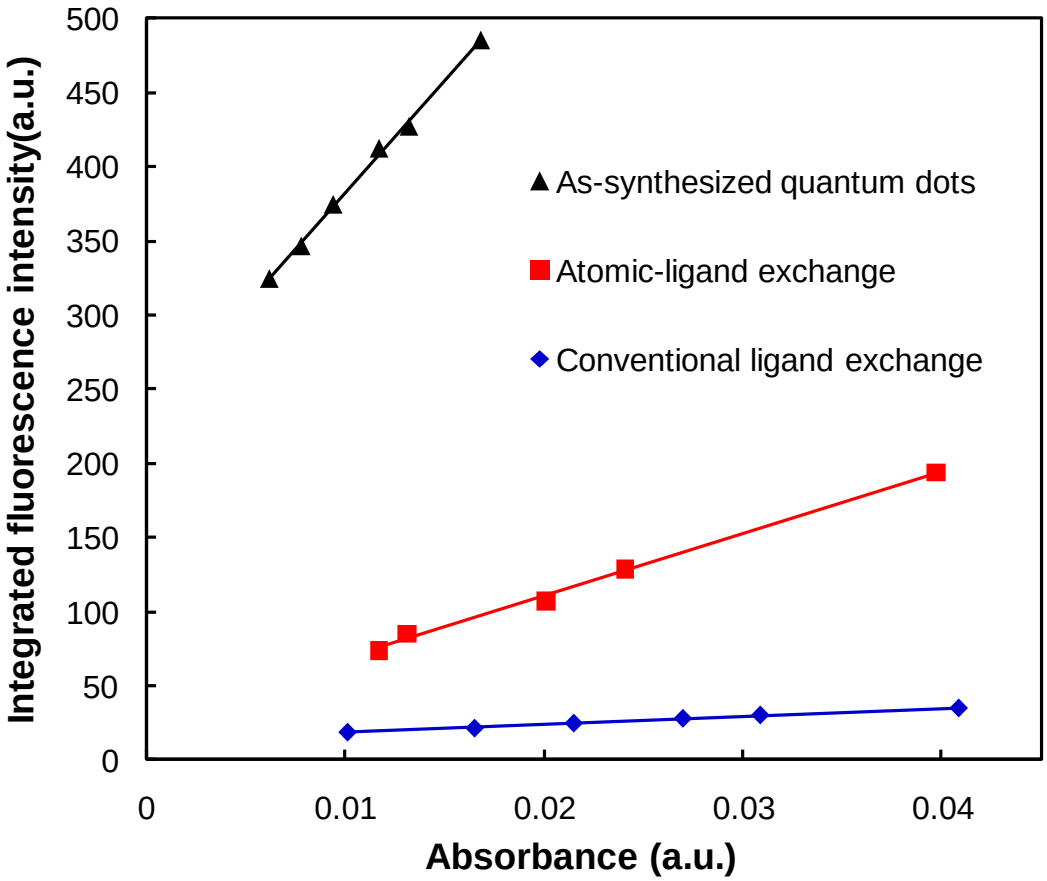

Figure 5.8 Fitting of fluorescence intensity (area of fluorescence spectrum) and peak absorption intensity for PbS QDs before and after ligand exchange

Table 5.1 Data from fluorescence intensity-absorbance linear fitting and quantum yield calculated according to given data

	Gradient	**R^2**	**Refractive index of solvent**	**Quantum yield**
As-synthesized QD (in toluene)	15142	0.9977	1.4969	87.2%
QD-conventional (in H_2O)	538	0.9957	1.4243	2.7%
QD-atomic ligand (in H_2O)	4215	0.9962	1.4243	22.0%

5.5 Controlling the atomic-ligand exchange reaction

To better understand the reaction in our atomic-ligand approach, reaction temperature during addition of Pb atom and degasification were controlled. For Pb atom attachment and ligand exchange, three temperatures were compared. The reactant feed was controlled at 1 g modified mPEG, 40 mg PbO and 5 mL DMF, and the solutions were stirred at room temperature (24ºC), 50ºC or 110ºC. No change of colour was observed in the solution at room temperature, yellow precipitation of PbO was easily observed at the bottom of the flask. For reaction at 50ºC, the solution showed slightly yellow colour, but large amount of PbO precipitation could still be found. When reacting at 110ºC the solution was yellow in colour after 2 hour reaction, and only trace amount of unreacted PbO was observed at the bottom of the flask, which was reasonable considering the excess amount of PbO added. After precipitation with diethyl ether and dry, both samples reacted at room temperature and 50ºC maintained the white colour of mPEG. For sample reacted at 110ºC yellow solid was obtained.

The atomic-ligand exchange reaction was carried out at 50ºC and 110ºC using PbO modified mPEG reacted at corresponding temperature. Although reaction at 110ºC was successful with high quantum yield, at 50ºC no QDs were observed in dried sample. This is believed to be due to the increased etching of QDs at elevated temperature. Because the Pb atom could not efficiently react with tri-dentate mPEG at 50ºC, large amount of remaining

carboxyl group exists in the ligand exchange reaction, which in turn causes surface etching of PbS QDs.

The initial attempt of ligand exchange was carried out in argon at 110ºC without degasification. Although the product showed brown in colour and is readily dispersed in H_2O, no absorption peak is observed (Figure 5.9 A). After including the degas step, absorption peak at 606 nm could be observed in absorption spectrum. TEM images of precipitated sample solution in H_2O were taken for reactions with and without degasification. Figure 5.9 B shows that PbS QDs are successfully exchanged into the aquatic solution without degassing. The disappearing of absorption peak for sample without degasification is possibly due to the surface oxidation. The elevated reaction temperature allows surface oxidation to take place rapidly, resulting in a large band gap insulating shell around the particles. Previous research on PbS solar cells has also supported this explanation. It has been pointed out that, by annealing the casted PbS layer in air or ozone, an insulating oxidation layer of PbO, $PbSO_3$ and $PbSO_4$ was formed outside the PbS particles, successfully quenching the PbS core.[79] However the fluorescence quenching of the particles should not result in the disappearing of absorption peaks, and the underlying reason for such observation is yet to be understood.

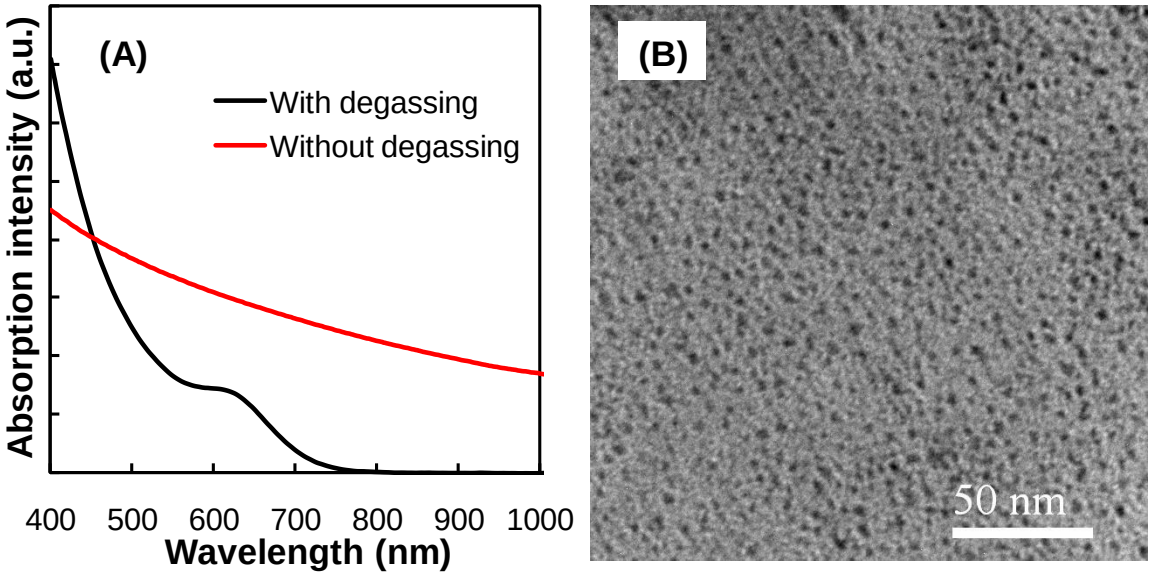

Figure 5.9 Effect of degassing on optical properties and morphology. (A) absorption spectra of PbS QDs using atomic-ligand approach with and without degassing; (B) TEM image of PbS QDs after atomic-ligand exchange without degassing, THF as solvent

5.6 Summary

A novel hydrophilic atomic-ligand exchange approach using tri-dentate mPEG is reported for PbS QDs, and this approach is compared with conventional ligand exchange method of mix and stir. QDs exchanged via atomic-ligand approach could easily disperse in various polar solvents including H_2O, ethanol and acetone, and the sample shows better dispersity in polymer comparing to conventional approach. It is found that by using the atomic-ligand approach the quantum yield of PbS QDs after ligand exchange reaches 22%, over 8 times that from conventional method. Reaction temperature and degasification are controlled for the atomic-ligand exchange reactions. Elevated temperature (above 110ºC) is found to be essential for effective Pb atom attachment. Degasification before ligand exchange is crucial

for this atomic-ligand method, as photoluminescence quenching is observed for reaction without degasification. This is believed to due to the surface oxidation of PbS QDs. Due to equipment limitation we are not able to further characterize the components of surface oxidation and the principles of photoluminescent quenching, which would be part of our future work. We will also apply this atomic-ligand exchange method for other organic ligands for possible application in PV devices.

Chapter 6 Conclusions and Recommendation

6.1 Conclusions

The work reported in this thesis has focused on the fundamental study of PbS QDs synthesis and properties modification. Based on the organometallic synthesis and chemistry modification, the process of particle growth was investigated and a novel ligand exchange strategy was introduced.

In this thesis hot-injection method was used to synthesize PbS QDs with absorption peaks from ~500 nm to 900 nm. The synthesized particles show narrow photoluminescence peaks with FWHM around 68 nm, which is comparable to the best reported results. By monitoring particle growth through time, the growth could be identified into three stages. The nucleation stage shows relatively unified absorption peak despite the temperature and reactant feed variation, possibly implying a critical particle size of around 2.1 nm in diameter for further growth. The particle growth stage follows a near logarithm trend with time, and by controlling the reaction temperature and reactant feed the dependency of reaction rate on these parameters were investigated, and an activation energy of ~29 kJ/mol was calculated. For the saturated stage where particle size reaches constant, the final particle size was observed to increase with reaction temperature and oleic acid feed, such dependency requires future study for better understanding.

To exchange surface ligand with other desired organics while preserving optical properties, a novel atomic-ligand approach was used. DTPA modified mPEG was used as the model hydrophilic ligand to transfer PbS QDs from toluene into aqua solution. The modification of mPEG with DTPA and the connection of Pb atoms on carboxyl groups were confirmed, and the proposed approach could successfully transfer QDs into H_2O solution. By comparing with traditional ligand exchange method, the atomic-ligand approach is found to allow better dispersion of nanoparticles in the polymer whereas phase separation is observed for nanoparticles exchanged with conventional method. We observe quantum yield of 22% in H_2O using atomic-ligand exchange method, nearly 8 folds of that of 2.7% via conventional method.

6.2 Future recommendation

Based on the research provided in this thesis, recommendations for further investigation of PbS application in polymer-based solar cells are as follows.

Well understood growing mechanism is the footstone for QDs size selection, therefore further investigation could be done on theoretical study of QD formation and particle growth. Getting a calculative relation between different reaction parameters and particle size would become a guideline for particle size control. Understanding the change of energy bands with particle size and reaction conditions will also be helpful for particle selection in PV application.

To apply QDs into PV devices, the atomic-ligand approach could be introduced to other ligands with various functional groups, enabling the QDs and polymers to form hybrids via solution blending, π-π stacking or covalent bonding. The effect of different attachment approaches could be compared, and the underlying mechanism for charge transfer between QDs and conjugated polymer requires better understanding.

REFERENCES

(1) Yang, H.; Yu, C. Z.; Song, Q. L.; Xia, Y. Y.; Li, F. Y.; Chen, Z. G.; Li, X. G.; Yi, T.; Huang, C. H. *Chemistry of Materials* **2006**, *18*, 5173.

(2) Gratzel, M. *Inorg Chem* **2005**, *44*, 6841.

(3) Liang, Y. Y.; Xu, Z.; Xia, J. B.; Tsai, S. T.; Wu, Y.; Li, G.; Ray, C.; Yu, L. P. *Adv Mater* **2010**, *22*, E135.

(4) Bozano, L.; Carter, S. A.; Scott, J. C.; Malliaras, G. G.; Brock, P. J. *Applied Physics Letters* **1999**, *74*, 1132.

(5) He, Z.; Zhong, C.; Huang, X.; Wong, W.-Y.; Wu, H.; Chen, L.; Su, S.; Cao, Y. *Advanced materials (Deerfield Beach, Fla.)* **2011**, *23*, 4636.

(6) Shen, Y. L.; Klein, M. W.; Jacobs, D. B.; Scott, J. C.; Malliaras, G. G. *Phys Rev Lett* **2001**, *86*, 3867.

(7) Scharber, M. C.; Wuhlbacher, D.; Koppe, M.; Denk, P.; Waldauf, C.; Heeger, A. J.; Brabec, C. L. *Adv Mater* **2006**, *18*, 789.

(8) Nelson, J. *Science* **2001**, *293*, 1059.

(9) McGehee, M. D. *Nature Photonics* **2009**, *3*, 250.

(10) Gunes, S.; Fritz, K. P.; Neugebauer, H.; Sariciftci, N. S.; Kumar, S.; Scholes, G. D. *Sol Energ Mat Sol C* **2007**, *91*, 420.

(11) Mukherjee, M.; Datta, A.; Chakravorty, D. *Applied Physics Letters* **1994**, *64*, 1159.

(12) Noone, K. M.; Subramaniyan, S.; Zhang, Q. F.; Cao, G. Z.; Jenekhe, S. A.; Ginger, D. S. *J Phys Chem C* **2011**, *115*, 24403.

(13) Saunders, B. R.; Turner, M. L. *Advances in Colloid and Interface Science* **2008**, *138*, 1.

(14) Chandrasekaran, J.; Nithyaprakash, D.; Ajjan, K. B.; Maruthamuthu, S.; Manoharan, D.; Kumar, S. *Renewable & Sustainable Energy Reviews* **2011**, *15*, 1228.

(15) Sariciftci, N. S.; Braun, D.; Zhang, C.; Srdanov, V. I.; Heeger, A. J.; Stucky, G.; Wudl, F. *Applied Physics Letters* **1993**, *62*, 585.

(16) Wudl, F. *Accounts Chem Res* **1992**, *25*, 157.

(17) Zhicai, H.; Chengmei, Z.; Shijian, S.; Miao, X.; Hongbin, W.; Yong, C. *Nature Photonics* **2012**, *6*.

(18) Liang, Y. Y.; Yu, L. P. *Accounts Chem Res* **2010**, *43*, 1227.

(19) Zhou, H.; Zhang, Y.; Seifter, J.; Collins, S.; Luo, C.; Bazan, G.; Nguyen, T.-Q.; Heeger, A. *Advanced materials (Deerfield Beach, Fla.)* **2013**, *25*, 1646.

(20) Triantou, D.; Soulis, S.; Koureli, S.; De Sio, A.; von Hauff, E. *J Appl Polym Sci* **2013**, *127*, 585.

(21) Ye, H.; Feng, L.; Xia, G.; Wei, Z.; Yu, G.; Jianping, Z.; Charles, C. H.; Thomas, P. R.; Jianhui, H. *Advanced Energy Materials* **2013**.

(22) Letian, D.; Jingbi, Y.; Jun, Y.; Chun-Chao, C.; Youjun, H.; Seiichiro, M.; Tom, M.; Keith, E.; Gang, L.; Yang, Y. *Nature Photonics* **2012**, *6*.

(23) Gan, Q.; Bartoli, F.; Kafafi, Z. *Advanced materials (Deerfield Beach, Fla.)* **2013**.

(24) Janssen, R.; Nelson, J. *Advanced materials (Deerfield Beach, Fla.)* **2013**, *25*, 1847.

(25) Chidichimo, G.; Filippelli, L. *International Journal of Photoenergy* **2010**.

(26) Kim, S.; Fisher, B.; Eisler, H.-J.; Bawendi, M. *J Am Chem Soc* **2003**, *125*, 11466.

(27) Nenadovic, M.; Comor, M.; Vasic…, V. *Journal of Physical …* **1990**.

(28) Trinh, M. T.; Polak, L.; Schins, J. M.; Houtepen, A. J.; Vaxenburg, R.; Maikov, G. I.; Grinbom, G.; Midgett, A. G.; Luther, J. M.; Beard, M. C.; Nozik, A. J.; Bonn, M.; Lifshitz, E.; Siebbeles, L. D. A. *Nano Letters* **2011**, *11*, 1623.

(29) Yin, Y.; Alivisatos, A. P. *Nature* **2005**, *437*, 664.

(30) Gao, F. M. *Applied Physics Letters* **2011**, *98*.

(31) Zunger, A. *Mrs Bull* **1998**, *23*, 35.

(32) Sargent, E. H. *Adv Mater* **2005**, *17*, 515.

(33) Wise, F. W. *Accounts Chem Res* **2000**, *33*, 773.

(34) Peng, X. G.; Manna, L.; Yang, W. D.; Wickham, J.; Scher, E.; Kadavanich, A.; Alivisatos, A. P. *Nature* **2000**, *404*, 59.

(35) Nootz, G.; Padilha, L. A.; Levina, L.; Sukhovatkin, V.; Webster, S.; Brzozowski, L.; Sargent, E. H.; Hagan, D. J.; Van Stryland, E. W. *Physical Review B* **2011**, *83*.

(36) Rakshit, T.; Mondal, S. P.; Manna, I.; Ray, S. K. *Acs Appl Mater Inter* **2012**, *4*, 6085.

(37) Scholes, G. D. *Adv Funct Mater* **2008**, *18*, 1157.

(38) Li, Q. C.; Kumar, V.; Li, Y.; Zhang, H. T.; Marks, T. J.; Chang, R. P. H. *Chemistry of Materials* **2005**, *17*, 1001.

(39) Li, Y.; Lu, P. F.; Jiang, M. L.; Dhakal, R.; Thapaliya, P.; Peng, Z. H.; Jha, B.; Yan, X. Z. *J Phys Chem C* **2012**, *116*, 25248.

(40) Sun, Y.; Fuge, G. M.; Fox, N. A.; Riley, D. J.; Ashfold, M. N. R. *Adv Mater* **2005**, *17*, 2477.

(41) Yin, B.; Liu, Q.; Yang, L. Y.; Wu, X. M.; Liu, Z. F.; Hua, Y. L.; Yin, S. G.; Chen, Y. S. *J Nanosci Nanotechno* **2010**, *10*, 1934.

(42) Guo, C. X.; Yang, H. B.; Sheng, Z. M.; Lu, Z. S.; Song, Q. L.; Li, C. M. *Angew Chem Int Edit* **2010**, *49*, 3014.

(43) Cheng, W. L.; Park, N. Y.; Walter, M. T.; Hartman, M. R.; Luo, D. *Nat. Nanotechnol.* **2008**, *3*, 682.

(44) Mor, G. K.; Varghese, O. K.; Paulose, M.; Grimes, C. A. *Adv Funct Mater* **2005**, *15*, 1291.

(45) Xia, Y. N.; Yang, P. D.; Sun, Y. G.; Wu, Y. Y.; Mayers, B.; Gates, B.; Yin, Y. D.; Kim, F.; Yan, Y. Q. *Adv Mater* **2003**, *15*, 353.

(46) Hallermann, M.; Kriegel, I.; Da Como, E.; Berger, J. M.; von Hauff, E.; Feldmann, J. *Adv Funct Mater* **2009**, *19*, 3662.

(47) Gunes, S.; Neugebauer, H.; Sariciftci, N. S. *Chemical Reviews* **2007**, *107*, 1324.

(48) Adikaari, A.; Dissanayake, D.; Silva, S. R. P. *Ieee Journal of Selected Topics in Quantum Electronics* **2010**, *16*, 1595.

(49) Mor, G. K.; Shankar, K.; Paulose, M.; Varghese, O. K.; Grimes, C. A. *Applied Physics Letters* **2007**, *91*.

(50) Kim, J. Y.; Kim, S. H.; Lee, H. H.; Lee, K.; Ma, W. L.; Gong, X.; Heeger, A. J. *Adv Mater* **2006**, *18*, 572.

(51) Burda, C.; Chen, X.; Narayanan, R.; El-Sayed, M. *Chemical Reviews* **2005**, *105*, 1025.

(52) Lianhua, Q.; Peng, Z. A.; Xiaogang, P. *Nano Letters* **2001**, *1*.

(53) Sharma, S. N.; Sharma, H.; Singh, G.; Shivaprasad, S. M. *Mater Chem Phys* **2008**, *110*, 471.

(54) Peng, Z.; Peng, X. *J Am Chem Soc* **2002**, *124*, 3343.

(55) Talapin, D. V.; Rogach, A. L.; Kornowski, A.; Haase, M.; Weller, H. *Nano Letters* **2001**, *1*, 207.

(56) Bullen, C. R.; Mulvaney, P. *Nano Letters* **2004**, *4*, 2303.

(57) Hines, M. A.; Scholes, G. D. *Adv Mater* **2003**, *15*, 1844.

(58) Murray, C.; Norris, D.; Bawendi, M. G. *J Am Chem Soc* **1993**, *115*, 8706.

(59) Vossmeyer, T.; Katsikas, L.; Giersig…, M. *The Journal of …* **1994**.

(60) Peng, Z. A.; Peng, X. G. *J Am Chem Soc* **2001**, *123*, 183.

(61) Yu, W. W.; Peng, X. G. *Angew Chem Int Edit* **2002**, *41*, 2368.

(62) Dethlefsen, J. R.; Dossing, A. *Nano Letters* **2011**, *11*, 1964.

(63) Dabbousi, B. O.; RodriguezViejo, J.; Mikulec, F. V.; Heine, J. R.; Mattoussi, H.; Ober, R.; Jensen, K. F.; Bawendi, M. G. *J Phys Chem B* **1997**, *101*, 9463.

(64) Kim, S.; Fisher, B.; Eisler, H. Y.; Bawendi, M. G. *Abstr Pap Am Chem S* **2002**, *224*, U443.

(65) Holder, E.; Tessler, N.; Rogach, A. L. *Journal of Materials Chemistry* **2008**, *18*, 1064.

(66) Liu, T. Y.; Li, M. J.; Ouyang, J. Y.; Zaman, M. B.; Wang, R. B.; Wu, X. H.; Yeh, C. S.; Lin, Q.; Yang, B.; Yu, K. *J Phys Chem C* **2009**, *113*, 2301.

(67) Fu, H.; Tsang, S.-W.; Zhang, Y.; Ouyang, J.; Lu, J.; Yu, K.; Tao, Y. *Chemistry of Materials* **2011**, *23*, 1805.

(68) Tiemann, M.; Marlow, F.; Hartikainen, J.; Weiss, O.; Linden, M. *J Phys Chem C* **2008**, *112*.

(69) Xue, B.; Cao, J.; Deng, D.; Xia, J.; Jin, J.; Qian, Z.; Gu, Y. *Journal of materials science. Materials in medicine* **2012**, *23*, 723.

(70) Barkhouse, D.; Pattantyus-Abraham, A.; Levina, L.; Sargent, E. *Acs Nano* **2008**, *2*, 2356.

(71) Rhodes, R.; O'Brien, P.; Saunders, B. R. *J Colloid Interf Sci* **2011**, *358*, 151.

(72) Thiry, M.; Boldt, K.; Nikolic, M.; Schulz, F.; Ijeh, M.; Panicker, A.; Vossmeyer, T.; Weller, H. *Acs Nano* **2011**, *5*, 4965.

(73) Streetman, B. G. *Solid state electronic devices / Ben G. Streetman and Sanjay Banerjee*; Englewood Cliffs, NJ : Prentice Hall: Englewood Cliffs, NJ, 2000.

(74) Breus, V. V.; Heyes, C. D.; Nienhaus, G. U. *J Phys Chem C* **2007**, *111*.

(75) Peet, J.; Kim, J. Y.; Coates, N. E.; Ma, W. L.; Moses, D.; Heeger, A. J.; Bazan, G. C. *Nature Materials* **2007**, *6*, 497.

(76) Yu, W.; Peng, X. *Angewandte Chemie (International ed. in English)* **2002**, *41*, 2368.

(77) Lingley, Z.; Lu, S. Y.; Madhukar, A. *Nano Letters* **2011**, *11*, 2887.

(78) Ip, A. H.; Thon, S. M.; Hoogland, S.; Voznyy, O.; Zhitomirsky, D.; Debnath, R.; Levina, L.; Rollny, L. R.; Carey, G. H.; Fischer, A.; Kemp, K. W.; Kramer, I. J.; Ning, Z. J.; Labelle, A. J.; Chou, K. W.; Amassian, A.; Sargent, E. H. *Nat. Nanotechnol.* **2012**, *7*, 577.

(79) Zhao, N.; Osedach, T. P.; Chang, L. Y.; Geyer, S. M.; Wanger, D.; Binda, M. T.; Arango, A. C.; Bawendi, M. G.; Bulovic, V. *Acs Nano* **2010**, *4*, 3743.

(80) Watt, A.; Thomsen, E.; Meredith, P.; Rubinsztein-Dunlop, H. *Chem Commun* **2004**, 2334.

(81) Langford, J. I.; Wilson, A. J. C. *J Appl Crystallogr* **1978**, *11*, 102.

(82) Cademartiri, L.; Montanari, E.; Calestani, G.; Migliori, A.; Guagliardi, A.; Ozin, G. A. *J Am Chem Soc* **2006**, *128*, 10337.

(83) Bakueva, L.; Gorelikov, I.; Musikhin, S.; Zhao, X. S.; Sargent, E. H.; Kumacheva, E. *Adv Mater* **2004**, *16*, 926.

(84) Huang, F.; Zhang, H. Z.; Banfield, J. F. *Nano Letters* **2003**, *3*, 373.

(85) Lin, W.; Fritz, K.; Guerin, G.; Bardajee, G. R.; Hinds, S.; Sukhovatkin, V.; Sargent, E. H.; Scholes, G. D.; Winnik, M. A. *Langmuir* **2008**, *24*, 8215.

(86) Ellingson, R. J.; Beard, M. C.; Johnson, J. C.; Yu, P. R.; Micic, O. I.; Nozik, A. J.; Shabaev, A.; Efros, A. L. *Nano Letters* **2005**, *5*, 865.